

Singlino-dominated dark matter in Z_3 -symmetric NMSSM

Haijing Zhou¹, Junjie Cao^{1,*}, Jingwei Lian, and Di Zhang¹

Physics Department, Henan Normal University, Xinxiang 453007, China

 (Received 11 February 2021; accepted 12 June 2021; published 13 July 2021)

Singlino-dominated dark matter properties are investigated in the Z_3 next-to-minimal supersymmetric Standard Model, producing superweak interactions with nucleons involved in dark matter direct-detection experiments. Approximate analytical formulas describing the dark matter abundance and cross section in the scattering with nucleons are used to illustrate a dependence on theoretical parameters in the neutralino and Higgs sectors. It is shown that the measured abundance requires a sizable singlet-doublet Higgs coupling parameter λ , while the experimental detection results prefer a small λ . The parameter space is then surveyed using a nest sampling technique guided by a likelihood function containing various observables in dark matter, Higgs, and B physics, such as the abundance and the scattering cross section. It is demonstrated that dark matter can achieve the correct abundance through $\tilde{\chi}_1^0 \tilde{\chi}_1^0 \rightarrow t\bar{t}$ or coannihilation with Higgsinos. The former process provides significantly larger Bayesian evidence than the latter, but this will be examined by the near-future PandaX-4T experiment. If the experiment shows no signs of dark matter, it will become highly disfavored. Furthermore, four cases are summarized to suppress dark matter scattering with nucleons, namely, a small λ and three kinds of cancellation between different contributions.

DOI: [10.1103/PhysRevD.104.015017](https://doi.org/10.1103/PhysRevD.104.015017)

I. INTRODUCTION

The 2012 discovery of the Higgs boson at the Large Hadron Collider (LHC) [1,2] confirmed the correctness of the Higgs mechanism as the origin of the masses of subatomic particles. However, the hierarchy problem caused by sizable radiative corrections to the Higgs mass term implies there should be new physics between the electroweak scale and the Planck scale. In addition, the Standard Model (SM) cannot explain the existence of dark matter (DM). However, current astronomical observations have confirmed that the Universe is composed of 27% DM [3,4]. Therefore, new DM particle candidates and new physics are required beyond the SM. Establishing the structural nature of DM is one of the most fundamental open questions in cosmology and particle physics.

Among multiple proposed theories, the most widely accepted are supersymmetry (SUSY) models with R -parity conservation, i.e., the minimal supersymmetric Standard Model (MSSM) [5,6] and the next-to-minimal supersymmetric Standard Model (NMSSM) [7–9], which provide elegant solutions to the hierarchy problem by introducing contributions from superpartners to the Higgs mass term. In

addition, R -parity conservation ensures that the lightest neutralino is a stable neutral particle if it is the lightest supersymmetric particle (LSP), and it may be an excellent DM candidate. The MSSM, the most economic realization of SUSY, exhibits several attractive features, but also includes some challenges (e.g., the “ μ problem” [10] and “little hierarchy problem” [11]) that have become exacerbated in recent years by the first run of the LHC experiments. This was particularly true for the uncomfortably large mass of the discovered Higgs boson $m_h \simeq 125$ GeV [12–20]. Alternatively, the NMSSM solves the μ problem by adding a singlet chiral superfield \hat{S} to the MSSM. In this process, the μ parameter is replaced by a dynamic quantity $\mu_{\text{eff}} = \lambda v_s$ when S develops a vacuum expectation value (VEV) v_s , the magnitude of which is naturally at the electroweak scale [8,9]. Furthermore, the SM-like Higgs squared mass can be enhanced by an additional tree-level contribution $\lambda^2 v^2 \sin^2 2\beta$ and the singlet-doublet Higgs mixing [12,13,15,17], where $\tan\beta \equiv v_u/v_d$ with v_u and v_d representing the VEVs of the doublet Higgs fields and $v^2 \equiv v_u^2 + v_d^2$. As a byproduct, the neutralino sector includes a fermionic partner of S (singlino) in addition to neutral electroweak gauginos (bino and wino) and the neutral fermionic partner of the Higgs doublets (Higgsinos). Since the coupling of a singlino field with SM particles may be very weak, this study focuses on the case of a singlino-dominated neutralino as a DM candidate [21–26]. This scenario is feasible when the Yukawa-like couplings satisfy $\lambda \geq 2\kappa$ and the gauginos are assumed to be heavier than the Higgsinos.

*junjiecao@alumni.itp.ac.cn

Published by the American Physical Society under the terms of the Creative Commons Attribution 4.0 International license. Further distribution of this work must maintain attribution to the author(s) and the published article's title, journal citation, and DOI. Funded by SCOAP³.

In the NMSSM, the Z boson mass is related to the Higgsino mass μ_{eff} , and a natural prediction of m_Z favors light Higgsinos up to several hundred GeV [27]. Generally, the NMSSM with $\mu_{\text{eff}} \lesssim 500$ GeV is considered to be a natural NMSSM [18,19,27–29]. However, given the constraints of recent experiments [e.g., the searches for electroweakinos [30–49], the WMAP/*Planck* experiments [3,4], and the DM direct-detection (DD) and indirect-detection experiments [50–54]], a large portion of the parameter space in the natural NMSSM has been strongly constrained. As a result, the following isolated and narrow parameter spaces with a singlino-dominated $\tilde{\chi}_1^0$ are preferred [55–58]:

- (1) $\lambda \simeq 2\kappa$ with $\lambda \lesssim 0.05$, where $\tilde{\chi}_1^0$ mainly coannihilates with Higgsinos to achieve the measured abundance [55].
- (2) $\kappa \sim 0.01$, $\lambda \lesssim 0.2$, and at least one light singlet-dominated Higgs boson [56]. Here, $\tilde{\chi}_1^0$ annihilates in certain funnel regions and the Higgsinos decay in a complex manner to satisfy the LHC constraints.

These conclusions are applicable for $|\mu_{\text{eff}}| \lesssim 500$ GeV, or equivalently, the fine-tuning criterion $\Delta m_Z \lesssim 50$, where Δm_Z defined in Ref. [59] parametrizes the sensitivity of m_Z to the SUSY parameters at the weak scale. Given this situation and the fact that the fine-tuning criteria lack a confirmed scientific basis and may reflect personal prejudice, we update the study by Cao *et al.* [55] to improve these conclusions. Specifically, we do not require Δm_Z to be less than 50 but impose the condition that $\mu_{\text{eff}} \leq 1$ TeV. We adopt an advanced MultiNest algorithm [60,61] to perform a sophisticated scan over the parameter space of the Z_3 -invariant NMSSM with a singlino-dominated DM. This algorithm is much more efficient than the other algorithms (e.g., the Markov chain method [62] adopted in Ref. [55]) in providing comprehensive information on the space to reveal the underlying physics, although it usually involves a tremendous amount of calculation. To the best of our knowledge, few researchers have used it to study the NMSSM phenomenology [63–68]. We also present a description of DM annihilation and the mechanisms used to suppress the DM nucleon scattering cross section through analytical formulas and numerical analysis. Some of the formulas are new, and some are consistent with excellent related works [69–73]. Evidently, such an analysis is helpful to understand the DM physics.

The remainder of this paper is organized as follows. In Sec. II, we briefly introduce the basic properties of the Z_3 -invariant NMSSM, including the Higgs and neutralino sections. We then demonstrate DM annihilation and scattering cross sections for singlino-dominated $\tilde{\chi}_1^0$ with nucleons using analytical formulas. In Sec. III, we provide a brief description of our scanning strategy. In Sec. IV, we investigate predictions for surviving samples and the properties of singlino-dominated DM scenarios to understand their distinctive features. Finally, Sec. V includes a discussion of the results and corresponding conclusions.

II. NEXT-TO-MINIMAL SUPERSYMMETRIC STANDARD MODEL

A. Fundamental NMSSM properties

As the simplest extension of the MSSM, the NMSSM includes one additional gauge singlet Higgs field \hat{S} . The associated superpotential can be expressed as follows [8,9]:

$$W_{\text{NMSSM}} = W_{\text{MSSM}} + \lambda \hat{S} \hat{H}_u \hat{H}_d + \frac{1}{3} \kappa \hat{S}^3, \quad (2.1)$$

where W_{MSSM} is the MSSM superpotential without the μ term, λ and κ are dimensionless parameters, and \hat{H}_u and \hat{H}_d are the common Higgs superfields. It is the most general R -parity-conserving superpotential satisfying a Z_3 discrete symmetry given the considered field content.

Assuming CP conservation, the Higgs sector of the Z_3 -NMSSM is determined by six parameters at the tree level [8,74]:

$$\lambda, \quad \kappa, \quad A_\lambda, \quad A_\kappa, \quad \mu_{\text{eff}}, \quad \tan\beta, \quad (2.2)$$

where A_λ and A_κ are the soft trilinear coefficients defined in Eq. (2.5) of Ref. [8]. In the base vectors, $H_{\text{SM}} \equiv \sin\beta \text{Re}[H_u^0] + \cos\beta \text{Re}[H_d^0]$, $H_{\text{NSM}} \equiv \cos\beta \text{Re}[H_u^0] - \sin\beta \text{Re}[H_d^0]$, and $H_S \equiv \text{Re}[S]$ for CP -even fields and $A_{\text{NSM}} \equiv \cos\beta \text{Im}[H_u^0] + \sin\beta \text{Im}[H_d^0]$ and $A_S \equiv \text{Im}[S]$ for CP -odd fields,¹ the three CP -even mass eigenstates $h_i = \{h, H, h_s\}$ and two CP -odd Higgs mass eigenstates $a_i = \{A_H, a_s\}$ are given as follows:

$$\begin{aligned} h_i &= V_{h_i}^{\text{SM}} H_{\text{SM}} + V_{h_i}^{\text{NSM}} H_{\text{NSM}} + V_{h_i}^S H_S, \\ a_i &= V_{a_i}^{\text{NSM}} A_{\text{NSM}} + V_{a_i}^S A_S, \end{aligned} \quad (2.3)$$

where V and V' represent the unitary matrices to diagonalize the corresponding Higgs squared mass matrix. In this work, we denote the physical Higgs state with the largest H_{SM} component by the symbol h , which is called the SM-like Higgs boson hereafter, and we denote the physical Higgs state with the largest non-SM doublet (singlet) component H_{NSM} (H_S) by H (h_s). We also denote the CP -even Higgs bosons by h_1, h_2 , and h_3 , with $m_{h_1} < m_{h_2} < m_{h_3}$. The latter notation is primarily for convenience. To date, the LHC experiments have measured the couplings of the discovered Higgs boson with about 10% uncertainty, and they revealed that the boson has roughly the same couplings as the SM Higgs boson [75,76]. These facts imply that $\sqrt{(V_h^{\text{NSM}})^2 + (V_h^S)^2} \lesssim 0.1$ and $|V_h^{\text{SM}}| \sim 1$.

In the Z_3 -NMSSM, mixtures of bino (\tilde{B}^0), wino (\tilde{W}^0), Higgsino ($\tilde{H}_{d,u}^0$), and singlino (\tilde{S}^0) fields form neutralinos. Assuming a basis of $\psi^0 = (-i\tilde{B}, -i\tilde{W}^0, \tilde{H}_d^0, \tilde{H}_u^0, \tilde{S})$ produces the following neutralino mass matrix [8]:

¹ H_u^0 , and H_d^0 denote the neutral component fields of the doublet scalar fields H_u and H_d , respectively.

$$\mathcal{M} = \begin{pmatrix} M_1 & 0 & -\frac{g_1 v_d}{\sqrt{2}} & \frac{g_1 v_u}{\sqrt{2}} & 0 \\ & M_2 & \frac{g_2 v_d}{\sqrt{2}} & -\frac{g_2 v_u}{\sqrt{2}} & 0 \\ & & 0 & -\mu_{\text{eff}} & -\lambda v_u \\ & & & 0 & -\lambda v_d \\ & & & & \frac{2\kappa}{\lambda} \mu_{\text{eff}} \end{pmatrix}, \quad (2.4)$$

where M_1 and M_2 denote the soft breaking masses of the bino and wino, respectively. Diagonalizing the mass matrix with a unitary matrix N yields five mass eigenstates (ordered by mass):

$$\tilde{\chi}_i^0 = N_{i1} \tilde{B}^0 + N_{i2} \tilde{W}_3^0 + N_{i3} \tilde{H}_d^0 + N_{i4} \tilde{H}_u^0 + N_{i5} \tilde{S}. \quad (2.5)$$

The lightest neutralino, $\tilde{\chi}_1^0$, acting as the DM candidate is the focus of this work.

In the limit that $|M_1|$ and $|M_2|$ are much larger than $|\mu_{\text{eff}}|$ and v , $\tilde{\chi}_1^0$ is approximated by

$$\tilde{\chi}_1^0 \simeq N_{13} \tilde{H}_d^0 + N_{14} \tilde{H}_u^0 + N_{15} \tilde{S}. \quad (2.6)$$

If $|\kappa/\lambda| < 1$, the dominant composition of $\tilde{\chi}_1^0$ is a singlino. In this case, κ is related to $m_{\tilde{\chi}_1^0}$ as [69,70]

$$\kappa = \frac{\lambda}{2\mu_{\text{eff}}} \left[m_{\tilde{\chi}_1^0} - \frac{\lambda^2 v^2 (m_{\tilde{\chi}_1^0} - \mu_{\text{eff}} \sin 2\beta)}{m_{\tilde{\chi}_1^0}^2 - \mu_{\text{eff}}^2} \right], \quad (2.7)$$

and the elements of the matrix N exhibit the following relationships [69–73]:

$$\frac{N_{13}}{N_{15}} = \frac{\lambda v}{\mu_{\text{eff}}} \frac{(m_{\tilde{\chi}_1^0}/\mu_{\text{eff}}) \sin \beta - \cos \beta}{1 - (m_{\tilde{\chi}_1^0}/\mu_{\text{eff}})^2}, \quad (2.8)$$

$$\frac{N_{14}}{N_{15}} = \frac{\lambda v}{\mu_{\text{eff}}} \frac{(m_{\tilde{\chi}_1^0}/\mu_{\text{eff}}) \cos \beta - \sin \beta}{1 - (m_{\tilde{\chi}_1^0}/\mu_{\text{eff}})^2}. \quad (2.9)$$

Thus,

$$N_{15}^2 \simeq \left(1 + \frac{N_{13}^2}{N_{15}^2} + \frac{N_{14}^2}{N_{15}^2} \right)^{-1} \frac{[1 - (m_{\tilde{\chi}_1^0}/\mu_{\text{eff}})^2]^2}{[(m_{\tilde{\chi}_1^0}/\mu_{\text{eff}})^2 - 2(m_{\tilde{\chi}_1^0}/\mu_{\text{eff}}) \sin 2\beta + 1](\lambda v/\mu_{\text{eff}})^2 + [1 - (m_{\tilde{\chi}_1^0}/\mu_{\text{eff}})^2]^2}. \quad (2.10)$$

The Higgsino and singlino fractions in $\tilde{\chi}_1^0$ can be defined as $Z_h = N_{13}^2 + N_{14}^2$ and $Z_s = N_{15}^2$, respectively. The ratio of Z_h to Z_s can then be expressed as follows:

$$\frac{Z_h}{Z_s} = \left(\frac{\lambda v}{\mu_{\text{eff}}} \right)^2 \frac{(m_{\tilde{\chi}_1^0}/\mu_{\text{eff}})^2 - 2(m_{\tilde{\chi}_1^0}/\mu_{\text{eff}}) \sin 2\beta + 1}{[1 - (m_{\tilde{\chi}_1^0}/\mu_{\text{eff}})^2]^2}. \quad (2.11)$$

This expression implies that a small λ can suppress the Higgsino fraction in $\tilde{\chi}_1^0$.

The couplings of DM to scalar Higgs states, the Z boson, and the Goldstone boson G^0 are included in the calculation of DM annihilation. They take the following form [8]:

$$\mathcal{L}_{\text{NMSSM}} \ni C_{\tilde{\chi}_1^0 \tilde{\chi}_1^0 Z} \bar{\tilde{\chi}}_1^0 \gamma^\mu \tilde{\chi}_1^0 + i C_{\tilde{\chi}_1^0 \tilde{\chi}_1^0 G^0} \bar{\tilde{\chi}}_1^0 \gamma_5 \tilde{\chi}_1^0 + C_{\tilde{\chi}_1^0 \tilde{\chi}_1^0 h_i} h_i \bar{\tilde{\chi}}_1^0 \tilde{\chi}_1^0 + i C_{\tilde{\chi}_1^0 \tilde{\chi}_1^0 a_i} a_i \bar{\tilde{\chi}}_1^0 \gamma_5 \tilde{\chi}_1^0,$$

where the coefficients are given by

$$C_{\tilde{\chi}_1^0 \tilde{\chi}_1^0 Z} \simeq \frac{m_Z}{\sqrt{2}v} \left(\frac{\lambda v}{\mu_{\text{eff}}} \right)^2 \frac{Z_s \cos 2\beta}{1 - (m_{\tilde{\chi}_1^0}/\mu_{\text{eff}})^2}, \quad (2.12)$$

$$C_{\tilde{\chi}_1^0 \tilde{\chi}_1^0 G^0} \simeq \frac{\sqrt{2}\mu_{\text{eff}}}{v} \left(\frac{\lambda v}{\mu_{\text{eff}}} \right)^2 \frac{Z_s (m_{\tilde{\chi}_1^0}/\mu_{\text{eff}}) \cos 2\beta}{1 - (m_{\tilde{\chi}_1^0}/\mu_{\text{eff}})^2}, \quad (2.13)$$

$$\begin{aligned}
 C_{\tilde{\chi}_1^0 \tilde{\chi}_1^0 h_i} &\simeq V_{h_i}^{\text{SM}} C_{\tilde{\chi}_1^0 \tilde{\chi}_1^0 H_{\text{SM}}} + V_{h_i}^{\text{NSM}} C_{\tilde{\chi}_1^0 \tilde{\chi}_1^0 H_{\text{NSM}}} + V_{h_i}^{\text{S}} C_{\tilde{\chi}_1^0 \tilde{\chi}_1^0 H_{\text{S}}} \\
 &\simeq \frac{\sqrt{2} \mu_{\text{eff}}}{v} \left(\frac{\lambda v}{\mu_{\text{eff}}} \right)^2 \frac{Z_s V_{h_i}^{\text{SM}} (m_{\tilde{\chi}_1^0} / \mu_{\text{eff}} - \sin 2\beta)}{1 - (m_{\tilde{\chi}_1^0} / \mu_{\text{eff}})^2} - \frac{\sqrt{2} \mu_{\text{eff}}}{v} \left(\frac{\lambda v}{\mu_{\text{eff}}} \right)^2 \frac{Z_s V_{h_i}^{\text{NSM}} \cos 2\beta}{1 - (m_{\tilde{\chi}_1^0} / \mu_{\text{eff}})^2} \\
 &\quad + \lambda \left(\frac{\lambda v}{\mu_{\text{eff}}} \right)^2 \frac{Z_s V_{h_i}^{\text{S}} \sin 2\beta}{\sqrt{2} [1 - (m_{\tilde{\chi}_1^0} / \mu_{\text{eff}})^2]} - \sqrt{2} \kappa Z_s V_{h_i}^{\text{S}} \left[1 + \left(\frac{\lambda v}{\mu_{\text{eff}}} \right)^2 \frac{2}{1 - (m_{\tilde{\chi}_1^0} / \mu_{\text{eff}})^2} \right], \tag{2.14}
 \end{aligned}$$

$$\begin{aligned}
 C_{\tilde{\chi}_1^0 \tilde{\chi}_1^0 a_i} &\simeq V_{a_i}^{\text{NSM}} C_{\tilde{\chi}_1^0 \tilde{\chi}_1^0 A_{\text{NSM}}} + V_{a_i}^{\text{S}} C_{\tilde{\chi}_1^0 \tilde{\chi}_1^0 A_{\text{S}}} \\
 &\simeq -\frac{\sqrt{2} \mu_{\text{eff}}}{v} \left(\frac{\lambda v}{\mu_{\text{eff}}} \right)^2 \frac{Z_s V_{a_i}^{\text{NSM}} (m_{\tilde{\chi}_1^0} / \mu_{\text{eff}} \sin 2\beta - 1)}{1 - (m_{\tilde{\chi}_1^0} / \mu_{\text{eff}})^2} \\
 &\quad + \lambda \left(\frac{\lambda v}{\mu_{\text{eff}}} \right)^2 \frac{Z_s V_{a_i}^{\text{S}} \sin 2\beta}{\sqrt{2} [1 - (m_{\tilde{\chi}_1^0} / \mu_{\text{eff}})^2]} - \sqrt{2} \kappa Z_s V_{a_i}^{\text{S}} \left[1 + \left(\frac{\lambda v}{\mu_{\text{eff}}} \right)^2 \frac{2}{1 - (m_{\tilde{\chi}_1^0} / \mu_{\text{eff}})^2} \right], \tag{2.15}
 \end{aligned}$$

where the approximation in Eq. (2.6) was applied. In addition, the coupling of a CP -even Higgs h_i to two quasidegenerate singlet CP -odd Higgs a_s , $\mathcal{L}_{\text{NMSSM}} \ni C_{h_i a_s a_s} h_i a_s a_s$, is relevant to our study. Its coefficient $C_{h_i a_s a_s}$ is given as follows [77,78]:

$$C_{h_i a_s a_s} \simeq \sqrt{2} \lambda v V_{h_i}^{\text{SM}} (\lambda + \kappa \sin 2\beta) + \sqrt{2} \lambda \kappa v V_{h_i}^{\text{NSM}} \cos 2\beta + \sqrt{2} V_{h_i}^{\text{S}} (2\kappa^2 v_s - \kappa A_\kappa). \tag{2.16}$$

In most cases, $C_{h_s a_s a_s} \gg C_{h_a a_s a_s}$, since $v_s \gg v$.

B. Dark matter relic density

In the NMSSM, the abundance of the singlino-dominated DM candidate ($\tilde{\chi}_1^0$) tends to be unacceptably large, due to small coupling effects with SM particles. However, such a candidate can still achieve the measured abundance [3,4] by a specific mechanism, e.g., via s -channel exchanges of gauge and Higgs bosons and t -channel exchanges of electroweakinos and sfermions. It can also be achieved through coannihilation with heavier states, such as sleptons, the next-to-lightest neutralino ($\tilde{\chi}_2^0$), or the lightest chargino ($\tilde{\chi}_1^\pm$).

The thermal abundance of the DM at the freeze-out temperature $T_F = m_{\tilde{\chi}_1^0} / x_F$ is given as follows [73]:

$$\Omega h^2 = 0.12 \left(\frac{80}{g_*} \right)^{1/2} \left(\frac{x_F}{25} \right) \left(\frac{2.3 \times 10^{-26} \text{ cm}^3/\text{s}}{\langle \sigma v \rangle_{x_F}} \right), \tag{2.17}$$

with a thermally averaged annihilation cross section $\langle \sigma v \rangle_{x_F} \equiv a + \frac{3b}{x_F}$. Dominant contributions to $\langle \sigma v \rangle_{x_F}$ in acquiring the measured abundance are discussed in Sec. 2.2 of Ref. [73]. The following conclusions were presented:

1) $\tilde{\chi}_1^0 \tilde{\chi}_1^0 \rightarrow t\bar{t}$ is usually the most crucial channel for the abundance when $m_{\tilde{\chi}_1^0} > m_t$. It proceeds through the s -channel exchanges of Higgs and Z bosons. Since the top quark is massive, the contribution from the Z boson's longitudinal polarization to $\langle \sigma v \rangle_{x_F}$ is important in this process when the Higgs mediators are far off shell. $\langle \sigma v \rangle_{x_F}$ can then be approximately expressed as follows:

$$\langle \sigma v \rangle_{x_F}^{\bar{t}t} \sim 2 \times 10^{-26} \frac{\text{cm}^3}{\text{s}} \left(\frac{|C_{\tilde{\chi}_1^0 \tilde{\chi}_1^0 G^0}|}{0.1} \right)^2 \left(\frac{m_{\tilde{\chi}_1^0}}{300 \text{ GeV}} \right)^{-2}. \tag{2.18}$$

The measured abundance $\Omega h^2 \sim 0.12$ [3,4] is achieved through the coupling of DM pairs to the Goldstone boson $|C_{\tilde{\chi}_1^0 \tilde{\chi}_1^0 G^0}| \sim 0.1$, which requires $\lambda \gtrsim 0.4$ according to Eq. (2.13).

2) $\tilde{\chi}_1^0 \tilde{\chi}_1^0 \rightarrow \Phi_i \Phi_j$ is another crucial annihilation process for the abundance, where Φ_i denotes a scalar or pseudoscalar Higgs mass eigenstate. Such processes occur via s -channel Higgs or Z boson exchange and t -channel neutralino exchange. Since $\tilde{\chi}_1^0 \tilde{\chi}_1^0 \rightarrow h_i h_j$ and $\tilde{\chi}_1^0 \tilde{\chi}_1^0 \rightarrow a_i a_j$ are p -wave suppressed [73], and because $C_{\tilde{\chi}_1^0 \tilde{\chi}_1^0 h_i}$ with $h_i = h, H$ in Eq. (2.14) and $C_{\tilde{\chi}_1^0 \tilde{\chi}_1^0 A_H}$ in Eq. (2.15) are usually smaller than 0.1, here we consider only the contribution from $\tilde{\chi}_1^0 \tilde{\chi}_1^0 \rightarrow h_s a_s$ to $\langle \sigma v \rangle_{x_F}$. $\langle \sigma v \rangle_{x_F}^{h_s a_s}$ is then given as follows [73,79]:

$$\begin{aligned}
 \langle \sigma v \rangle_{x_F}^{h_s a_s} &\simeq \frac{1}{64\pi m_{\tilde{\chi}_1^0}^2} \left\{ \left[1 - \frac{(m_{h_s} + m_{a_s})^2}{4m_{\tilde{\chi}_1^0}^2} \right] \right. \\
 &\quad \left. \times \left[1 - \frac{(m_{h_s} - m_{a_s})^2}{4m_{\tilde{\chi}_1^0}^2} \right] \right\}^{1/2} |\mathcal{A}_s + \mathcal{A}_t|^2, \tag{2.19}
 \end{aligned}$$

where the s - and t -channel contributions are approximated as

$$\begin{aligned}
 \mathcal{A}_s &\simeq \frac{-2m_{\tilde{\chi}_1^0} C_{\tilde{\chi}_1^0 \tilde{\chi}_1^0 a_s} C_{h_s a_s a_s}}{m_{a_s}^2 - 4m_{\tilde{\chi}_1^0}^2}, \\
 \mathcal{A}_t &\simeq -2C_{\tilde{\chi}_1^0 \tilde{\chi}_1^0 h_s} C_{\tilde{\chi}_1^0 \tilde{\chi}_1^0 a_s} \left[1 + \frac{2m_{a_s}^2}{4m_{\tilde{\chi}_1^0}^2 - (m_{h_s}^2 + m_{a_s}^2)} \right] \tag{2.20}
 \end{aligned}$$

if there are no resonant contributions.² According to Eqs. (2.14) and (2.15), if h_s , a_s , and $\tilde{\chi}_1^0$ are pure singlet states, then $|C_{\tilde{\chi}_1^0\tilde{\chi}_1^0 h_i}| = |C_{\tilde{\chi}_1^0\tilde{\chi}_1^0 a_i}| \sim \sqrt{2}|\kappa|$. The measured abundance then requires $\kappa \sim 0.15 \left(\frac{m_{\tilde{\chi}_1^0}}{300 \text{ GeV}}\right)^{1/2}$ in the case of $|\mathcal{A}_t| \gg |\mathcal{A}_s|$ [73]. Hence, it is evident that once the involved particle masses are fixed, the density is primarily determined by the parameter κ . However, because $\lambda > 2|\kappa|$ to ensure a singlino-dominated $\tilde{\chi}_1^0$, the measured abundance can set a lower bound on λ .

To date, the sensitivities of the XENON-1T experiments have reached the precision of 10^{-47} cm^2 for the spin-independent (SI) cross section [50] and 10^{-42} cm^2 for the spin-dependent (SD) cross section [51]. They have strongly restricted the $\lambda \gtrsim 0.3$ case (see the discussion about DM-nucleon scattering), which is preferred by the annihilations $\tilde{\chi}_1^0\tilde{\chi}_1^0 \rightarrow t\bar{t}$, $h_s a_s$ to account for the measured abundance. In addition, the LHC searches for new particles [30–49], and its precise measurement of the discovered scalar's properties [75,76], have reduced the parameter space accommodating light beyond-the-SM particles. This has a significant impact on the DM annihilation channels since they are usually accompanied with light particles to account for the abundance (see the discussion in Ref. [55]). Thus, the scenario preferred by the scan of Ref. [55] involves a singlino-dominated DM with $\lambda \lesssim 0.05$. In this case, an effective mechanism to obtain the measured abundance includes coannihilation with Higgsinos. The corresponding reaction is $\tilde{\chi}_i\tilde{\chi}_j \rightarrow XX'$, in which XX' denotes SM particles and $\tilde{\chi}_i\tilde{\chi}_j$ may be an LSP–next-to-LSP (NLSP) or NLSP–NLSP annihilation state (e.g., $\tilde{\chi}_1^0\tilde{\chi}_2^0$, $\tilde{\chi}_1^0\tilde{\chi}_1^+$, or $\tilde{\chi}_2^0\tilde{\chi}_1^+$). This mechanism is distinct in that the effective annihilation rate at a temperature T is very sensitive to the $\tilde{\chi}_1^0$ -Higgsino mass splitting [79,80], and even for a small λ and κ , it can still explain the measured abundance.³

²Note that the $\tilde{\chi}_i^0$ -mediated ($i \neq 1$) contribution to $\langle\sigma v\rangle_{\tilde{\chi}_1^0 h_s}^{h_s a_s}$ is less important than the $\tilde{\chi}_1^0$ -mediated contribution for two reasons. One is that, if $|\kappa|$ is comparable to λ , $|C_{\tilde{\chi}_1^0\tilde{\chi}_1^0 h_s}|$ and $|C_{\tilde{\chi}_1^0\tilde{\chi}_1^0 a_s}|$ are significantly smaller than $|C_{\tilde{\chi}_1^0\tilde{\chi}_1^0 h_s}|$ and $|C_{\tilde{\chi}_1^0\tilde{\chi}_1^0 a_s}|$, respectively. The other is that, since $m_{\tilde{\chi}_i^0} > m_{\tilde{\chi}_1^0}$, the former contribution is relatively suppressed by the propagator.

³Note that the coannihilation mechanism applies under the premise that $\tilde{\chi}_1^0$ and the Higgsinos remained in thermal equilibrium in the early Universe [79,80]. In the Z_3 -NMSSM, many processes, such as $\tilde{\chi}_1^0\tilde{\chi}_1^0 \leftrightarrow \tilde{\chi}_i\tilde{\chi}_j$, $\tilde{\chi}_1^0 X \leftrightarrow \tilde{\chi}_i X'$, and $\tilde{\chi}_i \leftrightarrow \tilde{\chi}_1^0 XX'$, could keep $\tilde{\chi}_1^0$ in chemical equilibrium with $\tilde{\chi}_i$, and the conversion rates of some of them might be enhanced if the mediator were around its mass shell. We add that maintaining the thermal equilibrium does not necessarily require the involved couplings to be moderately large. For example, the equilibrium condition was discussed in Eqs. (4.3) and (4.4) of Ref. [80] in the framework of the DM model ST11. It was found that the involved coupling may be as low as 10^{-4} to maintain the equilibrium.

C. DM-nucleon cross sections

Serving as a weakly interacting massive particle (WIMP), $\tilde{\chi}_1^0$ might be detected by measuring the recoil of a nucleus after an elastic scattering of $\tilde{\chi}_1^0$ on a nucleus takes place. In the nonrelativistic limit, only two different kinds of interactions between a neutralino and a nucleon need to be considered [81]: the SD interaction where the WIMP couples to the spin of the nucleus, and the SI interaction where the WIMP couples to the mass of the nucleus.

When $m_{\tilde{q}} \gtrsim 2 \text{ TeV}$, only the t -channel Z exchange diagram contributes significantly to the SD scattering cross section at the tree level, which is approximated by [82,83]

$$\sigma_{\tilde{\chi}_1^0-N}^{\text{SD}} \simeq C_N \times \left(\frac{C_{\tilde{\chi}_1^0\tilde{\chi}_1^0 Z}}{0.01}\right)^2, \quad (2.21)$$

with $N = p(n)$ denoting protons (neutrons) and $C_p \simeq 2.9 \times 10^{-41} \text{ cm}^2$ ($C_n \simeq 2.3 \times 10^{-41} \text{ cm}^2$) [71,72]. From the expression for $C_{\tilde{\chi}_1^0\tilde{\chi}_1^0 Z}$ in Eq. (2.12), it is evident that $\sigma_{\tilde{\chi}_1^0-N}^{\text{SD}}$ is proportional to $(\lambda v/\mu_{\text{eff}})^4$. Furthermore, in the coannihilation case, the degeneracy of $m_{\tilde{\chi}_1^0}$ and μ_{eff} leads to a minuscule denominator in Eq. (2.12), which requires a small value of $\lambda v/\mu_{\text{eff}}$ to satisfy the DM-DD experimental constraints.

In contrast, the SI scattering cross section in the heavy squark limit is dominated by a t -channel exchange of CP -even Higgs bosons h_i [84–87] and can be expressed as [88]

$$\sigma_{\tilde{\chi}_1^0-N}^{\text{SI}} = \frac{m_N^2}{2\pi v^2} \left(\frac{m_N m_{\tilde{\chi}_1^0}}{m_N + m_{\tilde{\chi}_1^0}}\right)^2 \left(\frac{1}{125 \text{ GeV}}\right)^4 \times \left\{ \sum_{h_i} [F_u^N(a_u)_{h_i} + F_d^N(a_d)_{h_i}] \right\}^2, \quad (2.22)$$

where m_N is the nucleon mass, $F_d^{(N)} = f_d^{(N)} + f_s^{(N)} + \frac{2}{27}f_G^{(N)}$ and $F_u^{(N)} = f_u^{(N)} + \frac{4}{27}f_G^{(N)}$ with $f_q^{(N)} = m_N^{-1} \langle N | m_q q \bar{q} | N \rangle$ ($q = u, d, s$) represent the normalized light quark contribution to the nucleon mass, and $f_G^{(N)} = 1 - \sum_{q=u,d,s} f_q^{(N)}$ influences other heavy quark mass fractions in nucleons [86,87]. In this study, the default settings for f_q^N were used in the micrOMEGAs package [85], and they predict $F_u^p \simeq F_u^n \simeq 0.15$ and $F_d^p \simeq F_d^n \simeq 0.13$. Hence, SI cross sections for DM-proton scattering and DM-neutron scattering are approximately equal (i.e., $\sigma_{\tilde{\chi}_1^0-p}^{\text{SI}} \simeq \sigma_{\tilde{\chi}_1^0-n}^{\text{SI}}$) [89]. The quantities $(a_u)_{h_i}$ and $(a_d)_{h_i}$ are defined by

$$(a_u)_{h_i} = \left(\frac{125 \text{ GeV}}{m_{h_i}}\right)^2 \left(V_{h_i}^{\text{SM}} + \frac{1}{\tan\beta} V_{h_i}^{\text{NSM}}\right) C_{\tilde{\chi}_1^0\tilde{\chi}_1^0 h_i}, \quad (2.23)$$

$$(a_d)_{h_i} = \left(\frac{125 \text{ GeV}}{m_{h_i}}\right)^2 (V_{h_i}^{\text{SM}} - \tan\beta V_{h_i}^{\text{NSM}}) C_{\tilde{\chi}_1^0\tilde{\chi}_1^0 h_i}. \quad (2.24)$$

Currently, non-SM doublet Higgs bosons H are preferred to be heavier than several hundreds of GeV in LHC experiments. In this case, the contribution from H to the SI cross section will be suppressed by $(a_q)_H^2 \propto 1/m_H^4$, and it is much smaller than that from h for a not exceedingly large $\tan\beta$. As such, the primary contribution to SI scattering comes from the t -channel exchange of SM-like Higgs bosons h and the singlet Higgs boson h_s . The latter contribution may be crucial when h_s is much lighter than h . Since the non-SM doublet components of h and h_s are approximately zero, $(a_u)_h + (a_u)_{h_s} \simeq (a_d)_h + (a_d)_{h_s} \equiv \mathcal{A}$, which can be expressed as

$$\mathcal{A} \simeq \left(\frac{125 \text{ GeV}}{m_h}\right)^2 V_h^{\text{SM}} C_{\tilde{\chi}_1^0 \tilde{\chi}_1^0 h} + \left(\frac{125 \text{ GeV}}{m_{h_s}}\right)^2 V_{h_s}^{\text{SM}} C_{\tilde{\chi}_1^0 \tilde{\chi}_1^0 h_s}, \quad (2.25)$$

where $C_{\tilde{\chi}_1^0 \tilde{\chi}_1^0 h}$ and $C_{\tilde{\chi}_1^0 \tilde{\chi}_1^0 h_s}$ are given by Eq. (2.14). Thus, the SI scattering cross section in Eq. (2.22) can be rewritten as

$$\begin{aligned} \sigma_{\tilde{\chi}_1^0-N}^{\text{SI}} &\simeq \frac{m_N^2}{2v^2\pi} \left(\frac{m_N m_{\tilde{\chi}_1^0}}{m_N + m_{\tilde{\chi}_1^0}}\right)^2 \left(\frac{1}{125 \text{ GeV}}\right)^4 \\ &\times (F_u^N + F_d^N)^2 \mathcal{A}^2 \sim 5 \times 10^{-45} \text{ cm}^2 \times \left(\frac{\mathcal{A}}{0.1}\right)^2. \end{aligned} \quad (2.26)$$

In these expressions, if only the contribution from a pure SM Higgs state is considered, \mathcal{A} can be simply expressed as

$$\mathcal{A} \sim \left(\frac{125 \text{ GeV}}{m_h}\right)^2 \frac{\sqrt{2}\lambda^2 v Z_s (m_{\tilde{\chi}_1^0}/\mu_{\text{eff}} - \sin 2\beta)}{\mu_{\text{eff}} [1 - (m_{\tilde{\chi}_1^0}/\mu_{\text{eff}})^2]}. \quad (2.27)$$

It is immediately evident that $\sigma_{\tilde{\chi}_1^0-N}^{\text{SI}}$ will vanish for $m_{\tilde{\chi}_1^0}/\mu_{\text{eff}} = \sin 2\beta$, which corresponds to a blind spot condition in Refs. [71,73,90].

The above analytical formulas for the SD and SI scattering cross sections suggest that $\sigma^{\text{SD}} \propto \left(\frac{\lambda v}{\mu_{\text{eff}}}\right)^2 \frac{1}{1 - (m_{\tilde{\chi}_1^0}/\mu_{\text{eff}})^2}$ and (by contrast) σ^{SI} depends on λ , μ_{eff} , and $m_{\tilde{\chi}_1^0}$ in a complex way. In general, a larger λ , a smaller μ_{eff} , and $m_{\tilde{\chi}_1^0}/\mu_{\text{eff}} \rightarrow 1$ will increase σ^{SI} and thus strengthen the DM-DD experimental constraints.

III. MODEL SCANS AND CONSTRAINTS

The NMSSMTools-5.4.1 package [77,91] was used to produce samples of singlino-dominated DM scenarios in the Z_3 -NMSSM and to model the corresponding features in detail.⁴ A sophisticated scan was first performed over the following ranges in the parameter space:

$$\begin{aligned} 0 < \lambda \leq 0.7, \quad |\kappa| \leq 0.7, \quad 1 \leq \tan\beta \leq 60, \quad 100 \text{ GeV} \leq \mu_{\text{eff}} \leq 1000 \text{ GeV}, \\ |A_\kappa| < 1 \text{ TeV}, \quad 0 < A_\lambda \leq 5 \text{ TeV}, \quad |A_t| \leq 5 \text{ TeV}, \quad |M_1| \leq 500 \text{ GeV}, \end{aligned} \quad (3.1)$$

in which all parameters were defined at the scale $Q = 1 \text{ TeV}$. Upper bounds of 0.7 were imposed on λ and $|\kappa|$ to maintain a perturbable theory up to the grand unification scale. A lower bound of 100 GeV was placed on μ_{eff} by the LEP search for electroweakinos [92], and an upper bound of 1000 GeV for μ_{eff} is large enough to allow us to consider various possibilities (see the discussion presented below). In addition, noting that the LHC search for SUSY prefers massive charged sparticles, the following assumptions were made concerning unimportant SUSY parameters. The electroweak gaugino masses were set to $M_2 = 2 \text{ TeV}$, and the gluino masses were set to $M_3 = 5 \text{ TeV}$. Soft SUSY-breaking parameters in the squarks sector were fixed at 2 TeV, excluding trilinear couplings $A_t = A_b$ used as free parameters to adjust the Higgs mass spectrum to coincide with relevant experimental

⁴The NMSSMTools package includes codes to compute various observables in Higgs physics, DM physics, B physics, and sparticle physics. In this sector, we only briefly introduce the calculation of the observables we are interested in.

measurements at the LHC. In addition, all slepton soft parameters were set to 2 TeV, as we did not want to explain the muon $g - 2$ anomaly. We also required $\lambda \geq 2|\kappa|$ in the scan to achieve a singlino-dominated $\tilde{\chi}_1^0$.

Specifically, the MultiNest algorithm [60,61] with flat distributions for all of the parameters in Eq. (3.1) and $n\text{live} = 20\,000$ were adopted during the scan to ensure that the conclusions were as complete as possible, and more than 20 000 CPU hours were spent on the calculations.⁵ Several constraints were imposed by constructing the

⁵The MultiNest sampling algorithm explores a high-dimensional parameter space by determining the iso-likelihood contour in each iteration with $n\text{live}$ active points. (The integer $n\text{live}$ is an input parameter of the algorithm, and it usually takes a value larger than 1000. In general, the larger value $n\text{live}$ adopts, the more accurate the scan result becomes.) [60,61] It is good at dealing with the case in which the samples' posterior distribution is multimodal or degenerate, which is frequently encountered in new physics studies. In contrast, the Markov chain method [62] is highly inefficient for such a situation, and thus, it usually provides incomplete information about the distribution.

following corresponding likelihood function to guide the process:

$$\mathcal{L} = \mathcal{L}_{m_h} \times \mathcal{L}_{h,\text{coupling}} \times \mathcal{L}_B \times \mathcal{L}_{\text{EW}} \times \mathcal{L}_{\Omega h^2} \times \mathcal{L}_{\text{DD}}, \quad (3.2)$$

where \mathcal{L}_{m_h} and $\mathcal{L}_{h,\text{coupling}}$ are likelihood functions for the experimentally measured SM-like Higgs boson mass and couplings, respectively. The computation of m_h included leading electroweak corrections, two-loop terms, and propagator corrections, as in Ref. [93]. Its experimental central value was taken as $m_h = 125.09$ GeV [20], and a total experimental and theoretical uncertainty of 3 GeV was assumed. $\mathcal{L}_{h,\text{coupling}}$ works in a seven-parameter κ -framework with related experimental measurements, such as the central values and uncertainties of the Higgs couplings and their correlation coefficients, taken from the ATLAS analysis, using 80 fb⁻¹ of data collected during the LHC Run II [75]. Some knowledge about probability and statistics was used in constructing $\mathcal{L}_{h,\text{coupling}}$ (see the introduction in Ref. [92]). \mathcal{L}_B is the likelihood function for the measurement of the branching ratio for the decays $B \rightarrow X_s \gamma$ and $B_s \rightarrow \mu^+ \mu^-$. These ratios were calculated using the formulas in Refs. [94,95], and their experimental values were taken from Ref. [92]. $\mathcal{L}_{\Omega h^2}$ and \mathcal{L}_{DD} are likelihood functions for the measured abundance from the WMAP/Planck experiments [3,4] and the detection of both SI and SD DM-nucleon scattering in the XENON-1T experiment [50,51]. Relevant quantities were calculated using the micrOMEGAs package [78,96–99]. In addition, \mathcal{L}_{EW} denotes a likelihood function for precision electroweak observables of ϵ_i ($i = 1, 2, 3$) [100–102] or, equivalently, S , T , and U parameters [103,104] calculated using the formulas from Ref. [105] and fitted to corresponding measurements by the procedure presented in Ref. [106]. Each of these likelihood functions was assumed to follow a Gaussian distribution, with explicit representations provided in Ref. [107].

The acquired samples were further refined using the following criteria: the SM-like Higgs mass was within the range of 122–128 GeV, the observed DM relic abundance was within $\pm 10\%$ of the measured central value $\Omega h^2 = 0.1187$ [4], the upper bound was a 90% confidence level of the XENON-1T experimental results of the SI cross section [50] and the SD cross section [51], and all other constraints implemented in NMSSMTools, including various B -physics observables in corresponding experimentally allowed ranges, were at the 2σ level. We also required the samples to satisfy $\chi_{\text{EW}}^2 \leq 7.8$ and $\chi_{h,\text{coupling}}^2 \leq 14.1$, which corresponded to 95% confidence level exclusion limits for three and seven degrees of freedom, respectively. Since a more significant deviation of the electroweak precision observables (the Higgs couplings) from their measured values would enhance χ_{EW}^2 ($\chi_{h,\text{coupling}}^2$), this requirement delineated

TABLE I. Signal of final state for the electroweakino pair production processes considered in this work. Relevant experimental analyses were performed using a simplified model by the ATLAS and CMS collaborations, and their results have been encoded in the SmodelS-1.2.3 [110].

Name	Simplified scenario	13 TeV	Signal of final state	Luminosity (fb ⁻¹)
CMS-SUS-17-010 [30] (arXiv:1807.07799)	$\tilde{\chi}_1^\pm \tilde{\chi}_1^\mp \rightarrow W^\pm \tilde{\chi}_1^0 W^\mp \tilde{\chi}_1^0$ $\tilde{\chi}_1^\pm \tilde{\chi}_1^\mp \rightarrow \nu \ell \ell \bar{\nu}$		$2\ell + E_{\text{T}}^{\text{miss}}$	35.9
CMS-SUS-17-009 [31] (arXiv:1806.05264)	$\tilde{\chi}_2^0 \tilde{\chi}_1^\pm \rightarrow W h(Z) \tilde{\chi}_1^0 \tilde{\chi}_1^\mp$ $\tilde{\chi}_2^0 \tilde{\chi}_1^\pm \rightarrow W^\pm \tilde{\chi}_1^0 h \tilde{\chi}_1^\mp$		$2\ell + E_{\text{T}}^{\text{miss}}$	35.9
CMS-SUS-17-004 [32] (arXiv:1801.03957)	$\tilde{\chi}_2^0 \tilde{\chi}_1^\pm \rightarrow \ell \bar{\nu} \ell \tilde{\chi}_1^\mp$		$n\ell(n >= 0) + nj(n >= 0) + E_{\text{T}}^{\text{miss}}$	35.9
CMS-SUS-16-045 [33] (arXiv:1709.00384)	$\tilde{\chi}_2^0 \tilde{\chi}_1^\pm \rightarrow \ell \bar{\nu} \ell \tilde{\chi}_1^\mp$		$1\ell 2b + E_{\text{T}}^{\text{miss}}$	35.9
CMS-SUSY-16-039 [34] (arXiv:1709.05406)	$\tilde{\chi}_2^0 \tilde{\chi}_1^\pm \rightarrow \tilde{\nu} \nu \ell \bar{\ell}$ $\tilde{\chi}_2^0 \tilde{\chi}_1^\pm \rightarrow \tilde{\nu} \nu \tau \bar{\tau}$		$n\ell(n > 0)(\tau) + E_{\text{T}}^{\text{miss}}$	35.9
CMS-SUS-16-034 [35] (arXiv:1709.08908)	$\tilde{\chi}_2^0 \tilde{\chi}_1^\pm \rightarrow W Z \tilde{\chi}_1^0 \tilde{\chi}_1^\mp$ $\tilde{\chi}_2^0 \tilde{\chi}_1^\pm \rightarrow W H \tilde{\chi}_1^0 \tilde{\chi}_1^\mp$ $\tilde{\chi}_2^0 \tilde{\chi}_1^\pm \rightarrow W \tilde{\chi}_1^0 Z(h) \tilde{\chi}_1^\mp$		$n\ell(n >= 2) + nj(n >= 1) E_{\text{T}}^{\text{miss}}$	35.9

(Table continued)

TABLE I. (Continued)

Name	Simplified scenario	Signal of final state	Luminosity (fb ⁻¹)
ATLAS-1803-02762 [36] (ATLAS-SUSY-2016-24)	$\tilde{\chi}_2^0 \tilde{\chi}_1^\pm \rightarrow W Z \tilde{\chi}_1^0 \tilde{\chi}_1^\pm$ $\tilde{\chi}_2^0 \tilde{\chi}_1^\pm \rightarrow \nu \tilde{\ell} \tilde{\ell}$ $\tilde{\chi}_1^\pm \tilde{\chi}_1^\mp \rightarrow \nu \tilde{\ell} \nu \tilde{\ell}$ $\tilde{\ell} \tilde{\ell}$	$n\ell (n >= 2) + E_{\text{T}}^{\text{miss}}$	36.1
ATLAS-1812-09432 [37] (ATLAS-SUSY-2017-01)	$\tilde{\chi}_2^0 \tilde{\chi}_1^\pm \rightarrow W h \tilde{\chi}_1^0 \tilde{\chi}_1^\pm$	$n\ell (n >= 0) + n_j (n >= 0) + nb (n >= 0) + n\gamma (n >= 0) + E_{\text{T}}^{\text{miss}}$	36.1
ATLAS-1806-02293 [38] (ATLAS-SUSY-2017-03)	$\tilde{\chi}_2^0 \tilde{\chi}_1^\pm \rightarrow W Z \tilde{\chi}_1^0 \tilde{\chi}_1^\pm$	$n\ell (n >= 2) + n_j (n >= 0) + E_{\text{T}}^{\text{miss}}$	36.1
ATLAS-1912-08479 [39] (ATLAS-SUSY-2018-06)	$\tilde{\chi}_2^0 \tilde{\chi}_1^\pm \rightarrow W (\rightarrow \nu) \tilde{\chi}_1^0 Z (\rightarrow \ell \ell) \tilde{\chi}_1^\pm$	$3\ell + E_{\text{T}}^{\text{miss}}$	139
ATLAS-1908-08215 [40] (ATLAS-SUSY-2018-32)	$\tilde{\ell} \tilde{\ell}$ $\tilde{\chi}_1^\pm \tilde{\chi}_1^\mp$	$2\ell + E_{\text{T}}^{\text{miss}}$	139
ATLAS-1909-09226 [41] (ATLAS-SUSY-2019-08)	$\tilde{\chi}_2^0 \tilde{\chi}_1^\pm \rightarrow W h \tilde{\chi}_1^0 \tilde{\chi}_1^\pm$	$1\ell + h (\rightarrow bb) + E_{\text{T}}^{\text{miss}}$	139
ATLAS-CONF-2013-035 [42]	$\tilde{\chi}_2^0 \tilde{\chi}_1^\pm \rightarrow Z^{(*)} \tilde{\chi}_1^0 W^{(*)} \tilde{\chi}_1^0$	$n\ell (n >= 2) + E_{\text{T}}^{\text{miss}}$	20.3
ATLAS-CONF-2013-049 [43] (arxiv:1801.01846)	$\tilde{\chi}_2^0 \tilde{\chi}_1^\pm \rightarrow \tilde{l}(\tilde{\nu}) \ell(\nu) \tilde{\ell}(\tilde{\nu}) \nu(\tilde{\ell})$ $\tilde{\ell} \tilde{\ell}$	$n\ell (n >= 2) + E_{\text{T}}^{\text{miss}}$	20.3
ATLAS-CONF-2013-093 [44]	$\tilde{\chi}_1^\pm \tilde{\chi}_1^\mp \rightarrow \tilde{\ell} \nu(\tilde{\nu} \ell)$	$2\ell + E_{\text{T}}^{\text{miss}}$	20.3
ATLAS-1403-5294 [45] (ATLAS-SUSY-2013-11)	$\tilde{\chi}_2^0 \tilde{\chi}_1^\pm \rightarrow W \tilde{\chi}_1^0 h \tilde{\chi}_1^\pm$ $\tilde{\chi}_1^\pm \tilde{\chi}_1^\mp \rightarrow \tilde{l}(\tilde{\nu}) \nu(l)$ $\tilde{\chi}_1^\pm \tilde{\chi}_1^\mp \rightarrow W \tilde{\chi}_1^0 W \tilde{\chi}_1^\pm$ $\tilde{\chi}_1^\pm \tilde{\chi}_2^0 \rightarrow W \tilde{\chi}_1^0 Z \tilde{\chi}_1^0$ $\tilde{\ell} \tilde{\ell}$	$1\ell + 2b + E_{\text{T}}^{\text{miss}}$ $n\ell (n >= 2) + E_{\text{T}}^{\text{miss}}$	20.3 20.3
ATLAS-1402-7029 [46] (ATLAS-SUSY-2013-12)	$\tilde{\chi}_2^0 \tilde{\chi}_1^\pm \rightarrow W \tilde{\chi}_1^0 Z \tilde{\chi}_1^\pm$ $\tilde{\chi}_2^0 \tilde{\chi}_1^\pm \rightarrow W \tilde{\chi}_1^0 h \tilde{\chi}_1^\pm$ $\tilde{\chi}_2^0 \tilde{\chi}_1^\pm \rightarrow \tilde{\ell} \tilde{\nu} \tilde{\ell}(\tilde{\nu} \nu), \tilde{\ell} \tilde{\ell} \nu \tilde{\ell}(\tilde{\nu} \nu)$ $\tilde{\chi}_2^0 \tilde{\chi}_1^\pm \rightarrow \tilde{\nu} \tilde{\nu} \tilde{\tau}(\tilde{\nu} \nu), \tilde{\tau} \tilde{\nu} \tilde{\tau}(\tilde{\nu} \nu)$	$3\ell(\tau) + E_{\text{T}}^{\text{miss}}$	20.3
ATLAS-1501-07110 [47] (ATLAS-SUSY-2013-23)	$\tilde{\chi}_2^0 \tilde{\chi}_1^\pm \rightarrow W \tilde{\chi}_1^0 h \tilde{\chi}_1^\pm$	$n\ell (n > 0) + n\gamma (n >= 0) + nb (n >= 0) + E_{\text{T}}^{\text{miss}}$	20.3
CMS-PAS-SUSY-12-022[48]	$\tilde{\chi}_2^0 \tilde{\chi}_1^\pm \rightarrow \tilde{\ell} \ell \tilde{\nu} \ell, \ell \tilde{\nu} \tilde{\ell}$ $\tilde{\chi}_1^0 \tilde{\chi}_1^\pm \rightarrow Z \tilde{\chi}_1^0 W \tilde{\chi}_1^\pm$ $\tilde{\chi}_2^0 \tilde{\chi}_3^0 \rightarrow Z \tilde{\chi}_1^0 Z \tilde{\chi}_1^0$ $\tilde{\chi}_1^\pm \tilde{\chi}_1^\mp \rightarrow \tilde{\ell} \tilde{\nu} \ell$ $\tilde{\ell} \tilde{\ell}$	$n\ell (n >= 2) + E_{\text{T}}^{\text{miss}}$	9.2
CMS-SUSY-13-006 [49]	$\tilde{\chi}_2^0 \tilde{\chi}_1^\pm \rightarrow \tilde{\ell} \ell \tilde{\nu} \ell, \ell \tilde{\nu} \tilde{\ell}$ $\tilde{\chi}_2^0 \tilde{\chi}_1^\pm \rightarrow Z \tilde{\chi}_1^0 W \tilde{\chi}_1^\pm$ $\tilde{\chi}_1^\pm \tilde{\chi}_1^\mp \rightarrow \tilde{\ell} \tilde{\nu} \ell$ $\tilde{\ell} \tilde{\ell}$	$n\ell (n >= 2) + E_{\text{T}}^{\text{miss}}$	19.5

the experimentally allowed range of these observables to further limit the Z_3 -NMSSM.

Constraints were also implemented from the LHC search for electroweakinos using the SModelS-1.2.3 code [108–110]. The final states listed in Table I from all of the electroweakino pair production processes were considered during this process.⁶ It is worth noting that a large portion of the samples satisfying these constraints were characterized by a small mass splitting between $\tilde{\chi}_1^0$ and $\tilde{\chi}_2^0$. However, the latest ATLAS analysis of the compressed mass spectra, acquired by searching soft dilepton signals [111], was not included in the SModelS-1.2.3 code. As such, the analysis constraints are validated in the Appendix, and they were applied to each sample by elaborate Monte Carlo simulations. We verified that they were very effective in excluding the coannihilation case. We illustrated this point in our recent publication [88].

We add that we did not consider constraints from indirect DM detection experiments (i.e., the Fermi-LAT search for DM annihilation from dwarf spheroidal galaxies) as they become loose for $m_{\tilde{\chi}_1^0} > 100$ GeV [54]. In addition, in the coannihilation case encountered in this work, the annihilation rate of singlino-dominated DM at present day is very small, which weakens the constraints.

IV. NUMERICAL RESULTS

A closer analysis suggested that the eventual surviving parameter space could be classified into the following three types:

- (1) Type-I samples: the lightest CP -even Higgs boson h_1 as the SM-like Higgs boson, $0.4 \lesssim \lambda \lesssim 0.7$, $0.13 \lesssim \kappa \lesssim 0.23$, $1.5 \lesssim \tan\beta \lesssim 6$, $450 \text{ GeV} \lesssim \mu_{\text{eff}} \lesssim 720 \text{ GeV}$, and the Bayesian evidence $\ln Z_1 = -24.2$. Due to the limited capability of the Markov chain algorithm, this type of samples was neglected in Ref. [55].
- (2) Type-II samples: the lightest CP -even Higgs boson h_1 as the SM-like Higgs boson, $\lambda \lesssim 0.08$, $-0.04 \lesssim \kappa < 0$ with $2|\kappa|/\lambda \simeq 1$, $4 \lesssim \tan\beta \lesssim 24$, $170 \text{ GeV} \lesssim \mu_{\text{eff}} \lesssim 420 \text{ GeV}$, and the Bayesian evidence $\ln Z_2 = -27.5$.
- (3) Type-III samples: the second lightest CP -even Higgs boson h_2 as the SM-like Higgs boson, $\lambda \lesssim 0.15$, $|\kappa| \lesssim 0.06$ with $2|\kappa|/\lambda \simeq 1$, $4.5 \lesssim \tan\beta \lesssim 32$,

⁶The concrete procedure to determine the limitation is as follows: we first determined the signal region (SR) with the largest expected sensitivity for a given sample, then we checked its R value defined by $R \equiv S/S_{95}^{\text{OBS}}$, where S stands for the number of signal events in the SR with the statistical uncertainty considered, and S_{95}^{OBS} denotes the observed limit at the 95% confidence level for the SR. Evidently, R represents the capability of the LHC in exploring a point. $R > 1$ implies that the point is excluded; otherwise, it is allowed.

$135 \text{ GeV} \lesssim \mu_{\text{eff}} \lesssim 260 \text{ GeV}$, and the Bayesian evidence $\ln Z_3 = -27.0$.

It is evident that the three types of parameter spaces are extremely narrow. The Bayesian evidence Z_i ($i = 1, 2, 3$) produced the Jeffreys' scales [112,113] $\delta_{12} \equiv \ln Z_1 - \ln Z_2 = 3.3$ and $\delta_{13} \equiv \ln Z_1 - \ln Z_3 = 2.8$. These results suggest that the considered experiments slightly preferred Type-I samples to Type-II and -III samples. However, as discussed below, Type-I samples will be examined by the near-future PandaX-4T experiment [114]. Furthermore, Type-II and -III samples share the following features in the parameter space: both λ and $|\kappa|$ are small, $2|\kappa|/\lambda \simeq 1$, and the Higgsinos are moderately light. These facts lead to the similarities of the Type-II and -III samples in many aspects of DM physics (see the discussions below for detailed similarities and differences). Nevertheless, they are still distinguished from each other in Higgs physics [13–18].

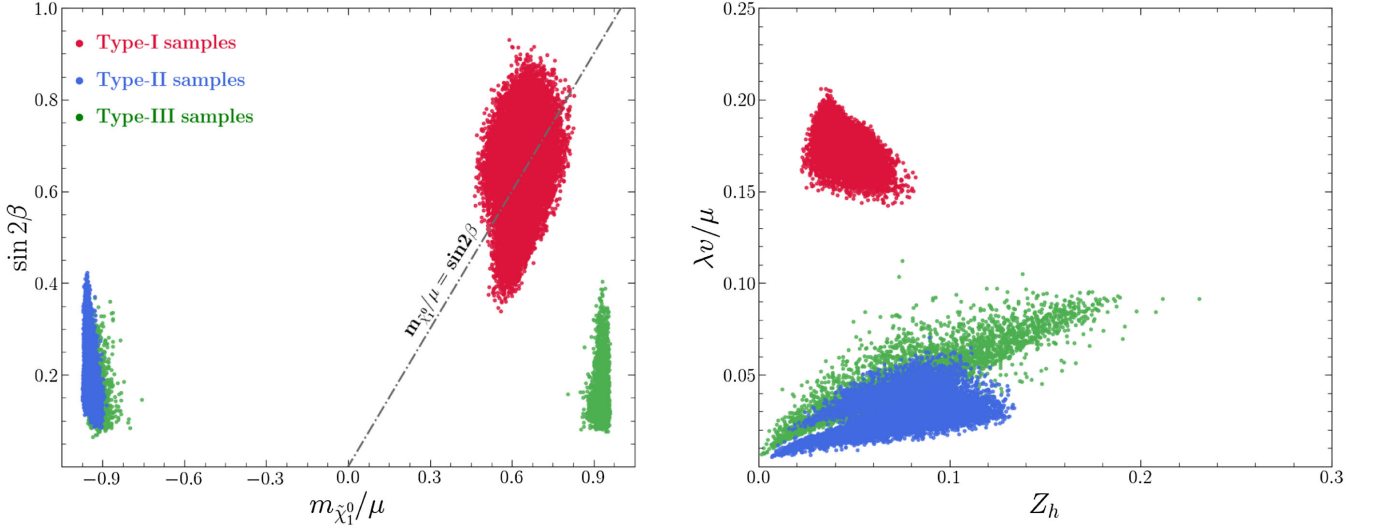
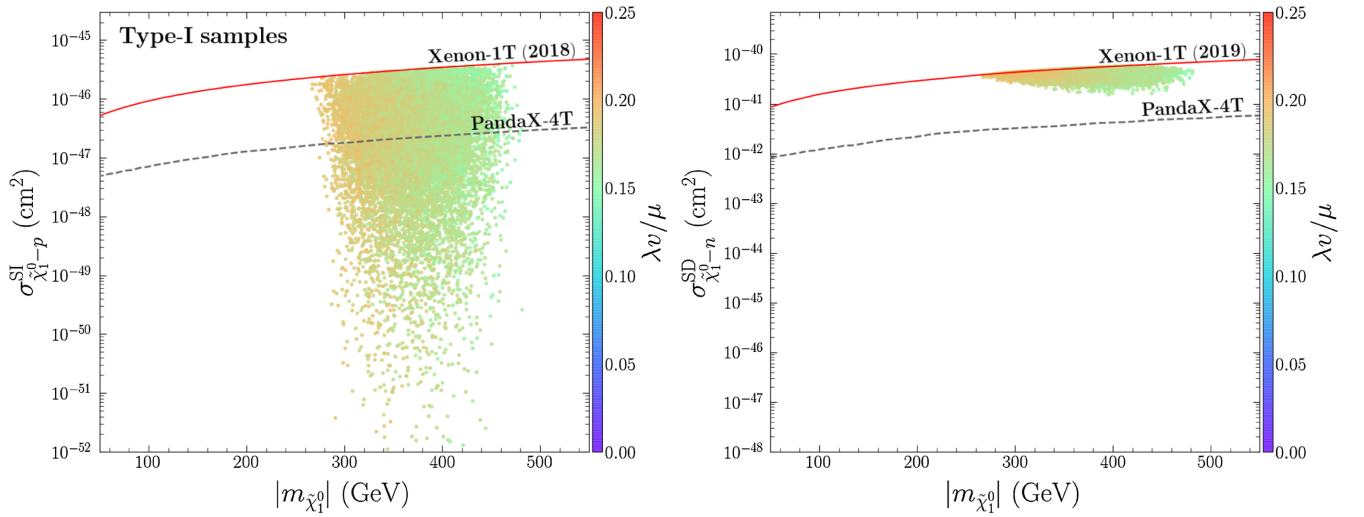
In the following, we investigate the characteristics of the singlino-dominated DM based on numerical results. In Fig. 1, Type-I, -II, and -III samples are projected on the $\sin 2\beta - m_{\tilde{\chi}_1^0}/\mu_{\text{eff}}$ and $\lambda v/\mu_{\text{eff}} - Z_h$ planes. In Figs. 2, 3, and 4, Type-I, -II, and -III samples are projected on the $\sigma_{\tilde{\chi}_1^0 - p}^{\text{SI}} - m_{\tilde{\chi}_1^0}$ and $\sigma_{\tilde{\chi}_1^0 - n}^{\text{SD}} - m_{\tilde{\chi}_1^0}$ planes, respectively, with different colors indicating the value of $\lambda v/\mu_{\text{eff}}$. In Table II, a selection of benchmark points are shown to further clarify features in each of the three scenarios.

The following points about Type-I samples can be determined from Figs. 1 and 2 and the point P_1 in Table II.

- (1) Type-I samples are characterized by a relatively large $\lambda v/\mu_{\text{eff}}$ ranging from 0.14 to 0.21 (see right panel of Fig. 1). This will increase the Higgsino composition in $\tilde{\chi}_1^0$ through Eq. (2.11) and the $\tilde{\chi}_1^0 \tilde{\chi}_1^0 Z$ coupling through Eq. (2.12). As indicated in the right panel of Fig. 2, the SD scattering rates are thus larger than $7 \times 10^{-42} \text{ cm}^2$, which are exceedingly close to the near-future PandaX-4T exclusion limit.
- (2) As shown in the left panel of Fig. 1, $m_{\tilde{\chi}_1^0}/\mu_{\text{eff}}$ and $\sin 2\beta$ are correlated by $m_{\tilde{\chi}_1^0}/\mu_{\text{eff}} \simeq \sin 2\beta$. In this case, $C_{\tilde{\chi}_1^0 \tilde{\chi}_1^0 H_{\text{SM}}}$ in Eq. (2.14) is suppressed by $m_{\tilde{\chi}_1^0}/\mu_{\text{eff}}$ and $\sin 2\beta$ cancellation, favored by the stringent bound of the XENON-1T experiment on the SI cross section. We further explore its implication by focusing on the point P_1 in Table II, which predicts the following four terms in Eq. (2.14):

$$C_{\tilde{\chi}_1^0 \tilde{\chi}_1^0 h} \simeq 0.2702 \times (0.6178 - 0.7647) + 0.0 - 0.0029 + 0.0465 \sim 0.0027, \quad (4.1)$$

$$C_{\tilde{\chi}_1^0 \tilde{\chi}_1^0 h_s} \simeq -0.006 - 0.0 + 0.0183 - 0.312 \sim -0.2997. \quad (4.2)$$


 FIG. 1. Type-I, -II, and -III samples projected on the $\sin 2\beta - m_{\tilde{\chi}_1^0}/\mu_{\text{eff}}$ and $\lambda v/\mu_{\text{eff}} - Z_h$ planes.

 FIG. 2. Type-I samples projected on the $\sigma_{\tilde{\chi}_1^0-p}^{\text{SI}} - m_{\tilde{\chi}_1^0}$ and $\sigma_{\tilde{\chi}_1^0-n}^{\text{SD}} - m_{\tilde{\chi}_1^0}$ planes. The color bar represents the values of $\lambda v/\mu_{\text{eff}}$. The solid line represents the current exclusion bound of the XENON-1T experiment on the cross section and the dashed line denotes the projected sensitivity of the near-future PandaX-4T experiment.

The two contributions in Eq. (2.25) are as follows:

$$\mathcal{A} \simeq 0.0027 - 0.0036 \sim -0.0009. \quad (4.3)$$

These results show that, besides the mentioned cancellation, there is a strong offsetting effect between the first and fourth terms within the $\tilde{\chi}_1^0 \tilde{\chi}_1^0 h$ coupling itself (i.e., cancellation between $C_{\tilde{\chi}_1^0 \tilde{\chi}_1^0 H_{\text{SM}}}$ and $C_{\tilde{\chi}_1^0 \tilde{\chi}_1^0 H_S}$ terms in $C_{\tilde{\chi}_1^0 \tilde{\chi}_1^0 h}$) and a strong cancellation between the two contributions to the SI cross section from h and h_s . These accidental cancellations result in $\sigma_{\tilde{\chi}_1^0-p}^{\text{SI}} \sim 10^{-49} \text{ cm}^2$. In contrast, $\sigma_{\tilde{\chi}_1^0-p}^{\text{SI}}$ would be around 10^{-42} cm^2 without them. This feature explains the SI cross section for Type-I

samples possibly being as low as 10^{-50} cm^2 , as shown in the left panel of Fig. 2.

- (3) Based on $m_{\tilde{\chi}_1^0}/\mu$, $\lambda v/\mu$, $\sin 2\beta$, and Z_h in Fig. 1, it is usually predicted that $C_{\tilde{\chi}_1^0 \tilde{\chi}_1^0 G^0} \sim 0.1$ by Eq. (2.13) and $\langle \sigma v \rangle_{x_F}^{\tilde{t}\tilde{t}} \sim 10^{-26} \text{ cm}^3 \text{ s}^{-1}$ by Eq. (2.18). This implies that $\tilde{\chi}_1^0 \tilde{\chi}_1^0 \rightarrow \tilde{t}\tilde{t}$ played a significant role in determining the abundance. Concerning the point P1 in Table II, we found $C_{\tilde{\chi}_1^0 \tilde{\chi}_1^0 G^0} \simeq -0.108$ and $\langle \sigma v \rangle_{x_F}^{\tilde{t}\tilde{t}} \simeq 1.2 \times 10^{-26} \text{ cm}^3 \text{ s}^{-1}$, indicating that the annihilation contributed to the total annihilation rate by about 52%. We also obtained $\langle \sigma v \rangle_{x_F}^{h_s a_s} \simeq 3.4 \times 10^{-27} \text{ cm}^3 \text{ s}^{-1}$ by Eq. (2.19), which means that $\tilde{\chi}_1^0 \tilde{\chi}_1^0 \rightarrow h_s a_s$ contributed to the total rate by 15%. We add that our estimation roughly agrees with the

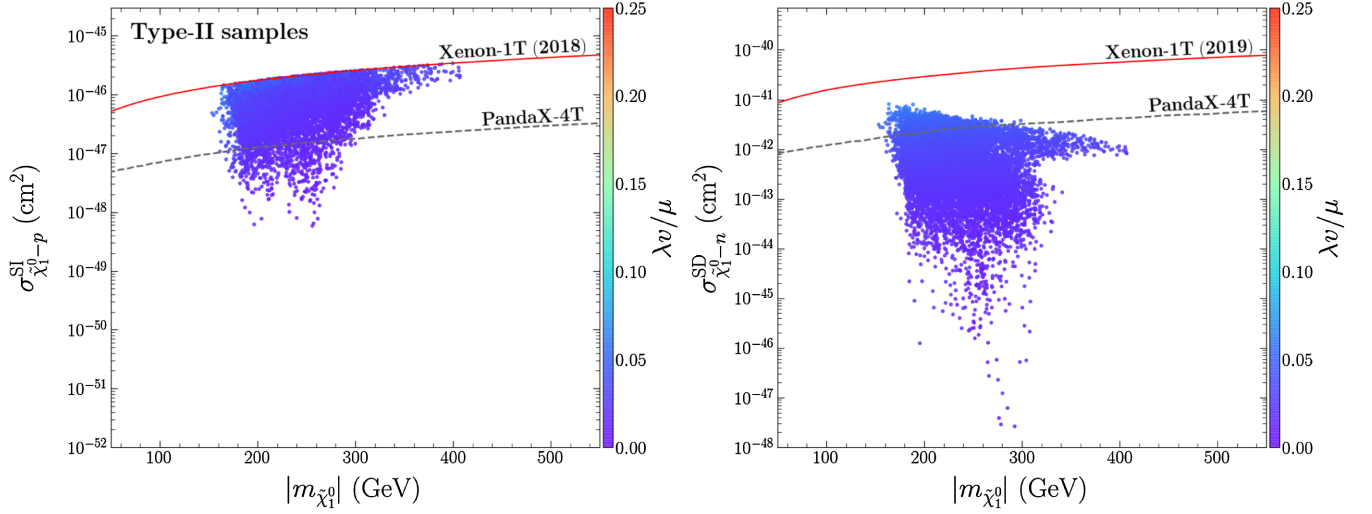


FIG. 3. Same plots as in Fig. 2, but for the results of the Type-II samples.

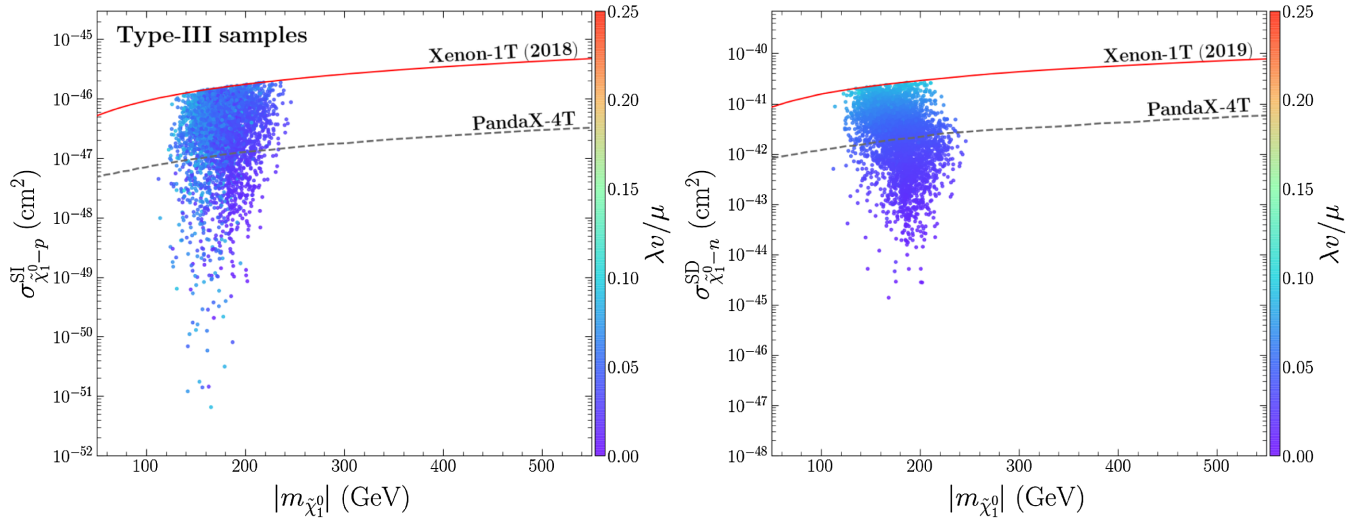


FIG. 4. Same plot as in Fig. 2, but for the results of the Type-III samples.

results in Table II, calculated by the micrOMEGAS package.

Next we consider Type-II samples. Figures 1 and 3 demonstrate the following features:

- (1) $\lambda v / \mu_{\text{eff}} \lesssim 0.06$ and $-0.95 \lesssim m_{\tilde{\chi}_1^0} / \mu_{\text{eff}} \lesssim -0.90$, which imply that

$$\begin{aligned} |C_{\tilde{\chi}_1^0 \tilde{\chi}_1^0 Z}| &\lesssim 2.4 \times (\lambda v / \mu_{\text{eff}})^2 < 0.009, \\ \sigma_{\tilde{\chi}_1^0-n}^{\text{SD}} / \text{cm}^2 &\lesssim 1.3 \times 10^{-36} \times (\lambda v / \mu_{\text{eff}})^4 < 1.7 \times 10^{-41} \end{aligned} \quad (4.4)$$

by Eq. (2.12) and (2.21), respectively. This feature is shown in the right panel of Fig. 3.

- (2) As indicated in the left panel of Fig. 1, $m_{\tilde{\chi}_1^0} / \mu_{\text{eff}}$ and $\sin 2\beta$ are of opposite sign, and thus their contributions to $C_{\tilde{\chi}_1^0 \tilde{\chi}_1^0 H_{\text{SM}}}$ in Eq. (2.14) do not cancel each

other. This implies that both $C_{\tilde{\chi}_1^0 \tilde{\chi}_1^0 h}$ and \mathcal{A} in Eq. (2.25) are mainly contributed by $C_{\tilde{\chi}_1^0 \tilde{\chi}_1^0 H_{\text{SM}}}$. Consequently, $\sigma_{\tilde{\chi}_1^0-p}^{\text{SI}}$ in Eq. (2.26) is approximated by

$$\sigma_{\tilde{\chi}_1^0-p}^{\text{SI}} \simeq 5 \times 10^{-45} \text{ cm}^2 \times \left(\frac{C_{\tilde{\chi}_1^0 \tilde{\chi}_1^0 H_{\text{SM}}}}{0.1} \right)^2, \quad (4.5)$$

where $C_{\tilde{\chi}_1^0 \tilde{\chi}_1^0 H_{\text{SM}}} \simeq (4-10) \times \sqrt{2} \lambda (\lambda v / \mu_{\text{eff}})$.⁷ This approximation reflects the relation $\sigma_{\tilde{\chi}_1^0-p}^{\text{SI}} \propto \lambda^4$. For a small λ , the cross section may be as low as 10^{-48} cm^2 , as shown in the left panel of Fig. 3.

⁷It is noticeable that the enhancement coefficient 4–10 comes from the factor $1/\{1 - (m_{\tilde{\chi}_1^0} / \mu_{\text{eff}})^2\}$ in Eq. (2.14). This is a common characteristic for the Type-II and -III samples.

TABLE II. Benchmark points satisfying various experimental constraints. Mass parameters are in units of GeV, and the DM-nucleon scattering cross sections are in units of cm^2 . The number preceding each annihilation process represents its fraction of contributions to the total DM annihilation cross section at the freeze-out temperature. Dots include the information of the decay modes with smaller branching ratios.

	SM-like Higgs: h_1		SM-like Higgs: h_2					
	P_1	P_2	P_3	P_4				
λ	0.696	0.028	0.108	9.64×10^{-3}				
κ	0.208	-0.013	0.048	-4.2×10^{-3}				
$\tan \beta$	2.15	7.2	12.8	9.9				
μ_{eff}	683.7	227.8	206.1	164.4				
A_t	-2734	2754	-3394	-3510				
A_λ	1128	3908	3125	1142				
A_κ	-28.3	24.4	-323.1	147.3				
M_1	-471.3	-418.2	-484.7	211.8				
$m_{\tilde{\chi}_1^0}$	422.4	-216.5	181.9	-148.6				
$m_{\tilde{\chi}_2^0}$	-473.7	-233.0	213.2	151.9				
$m_{\tilde{\chi}_3^0}$	702.3	234.5	-215.1	-174.5				
$m_{\tilde{\chi}_4^\pm}$	694.9	233.2	211.4	170.4				
N_{13}	-0.035	-0.164	-0.32	-0.032				
N_{14}	0.176	-0.171	-0.35	-0.038				
N_{15}	0.984	0.971	0.87	0.999				
Z_h	0.032	0.056	0.23	0.003				
Z_S	0.968	0.943	0.76	0.997				
m_{h_1}	124.6	125.2	64.2	100.7				
m_{h_2}	440.4	206.5	126.7	125.3				
m_{h_3}	1536	2532	2905	1311				
m_{a_1}	178.0	88.1	298.0	178.4				
m_{a_2}	1536	2532	2905	1311				
$V_{h_1}^{\text{NSM}}, V_{h_2}^{\text{NSM}}$	0.0, -0.05	-0.0, -0.0	-0.0, -0.0	-0.0, -0.0				
$V_{h_1}^{\text{SM}}, V_{h_2}^{\text{SM}}$	0.99, 0.15	0.99, -0.11	0.147, 0.989	0.04, 0.999				
$V_{h_1}^{\text{S}}, V_{h_2}^{\text{S}}$	-0.15, 0.99	0.11, 0.99	0.989, -0.147	0.999, -0.04				
$V_{a_1}^{\text{NSM}}, V_{a_1}^{\text{S}}$	-0.03, 1.0	-0.0, 1.0	-0.0, 1.0	-0.0, 1.0				
$\sigma_{\tilde{\chi}_1^0 - p}^{\text{SI}}$	4.2×10^{-49}	3.1×10^{-47}	8.89×10^{-47}	2.67×10^{-49}				
$\sigma_{\tilde{\chi}_1^0 - n}^{\text{SD}}$	3.0×10^{-41}	2.94×10^{-43}	2.23×10^{-41}	6.57×10^{-45}				
Ωh^2	0.118	0.109	0.12	0.108				
annihilation channels	68.4%	$\tilde{\chi}_1^0 \tilde{\chi}_1^0 \rightarrow t\bar{t}$	14.0%	$\tilde{\chi}_2^0 \tilde{\chi}_1^+ \rightarrow u\bar{d}$	28.7%	$\tilde{\chi}_1^0 \tilde{\chi}_1^0 \rightarrow W^+ W^-$	35.0%	$\tilde{\chi}_2^0 \tilde{\chi}_2^0 \rightarrow W^+ W^-$
	19.4%	$\rightarrow h_s a_s$	5.4%	$\rightarrow \nu_l \bar{l}$	22.0%	$\rightarrow ZZ$	25.4%	$\rightarrow ZZ$
	5.0%	$\rightarrow h_{sm} a_s$	13.0%	$\tilde{\chi}_3^0 \tilde{\chi}_1^+ \rightarrow u\bar{d}$	17.6%	$\rightarrow t\bar{t}$	16.2%	$\tilde{\chi}_2^0 \tilde{\chi}_1^+ \rightarrow u\bar{d}$
	2.2%	$\rightarrow W^+ W^-$	4.8%	$\rightarrow \nu_l \bar{l}$	13.0%	$\tilde{\chi}_1^0 \tilde{\chi}_1^+ \rightarrow u\bar{d}$	6.6%	$\rightarrow \nu_l \bar{l}$
	11.4%	$\tilde{\chi}_1^0 \tilde{\chi}_1^+ \rightarrow u\bar{d}$	4.8%	$\rightarrow \nu_l \bar{l}$	4.1%	$\tilde{\chi}_2^0 \tilde{\chi}_3^0 \rightarrow q\bar{q}$
			4.2%	$\rightarrow \nu_l \bar{l}$	3.8%	$\tilde{\chi}_1^0 \tilde{\chi}_3^0 \rightarrow q\bar{q}$	1.2%	$\rightarrow \nu_l \bar{\nu}_l$
			6.8%	$\tilde{\chi}_2^0 \tilde{\chi}_3^0 \rightarrow q\bar{q}$	3.6%	$\tilde{\chi}_1^0 \tilde{\chi}_2^0 \rightarrow q\bar{q}$
			1.8%	$\rightarrow \nu_l \bar{\nu}_l$		
			7.8%	$\tilde{\chi}_1^+ \tilde{\chi}_1^- \rightarrow q\bar{q}$				
			2.7%	$\rightarrow l\bar{l}$				
			2.2%	$\rightarrow W^+ W^-$				
			5.7%	$\tilde{\chi}_1^0 \tilde{\chi}_3^0 \rightarrow q\bar{q}$				
			1.5%	$\rightarrow \nu_l \bar{\nu}_l$				
						

We add that the SI cross sections in Fig. 3 are larger than $3 \times 10^{-49} \text{ cm}^2$ because smaller cross sections require smaller values of λ , which are not readily available since Bayesian evidence is suppressed significantly. We also add that the characteristics of $\sigma_{\tilde{\chi}_1^0 - p}^{\text{SI}}$ for the Type-I and -II samples are different because $\sigma_{\tilde{\chi}_1^0 - p}^{\text{SI}}$ has no significant cancellation effect in the latter case. Furthermore, we verified the approximation for $\sigma_{\tilde{\chi}_1^0 - p}^{\text{SI}}$ by considering the point P_2 in Table II. The four terms in Eq. (2.14) and the two contributions in Eq. (2.25) were as follows:

$$C_{\tilde{\chi}_1^0 \tilde{\chi}_1^0 h} \simeq -0.01 + 0.0 + 0.0 + 0.002 \sim -0.008, \\ \mathcal{A} \simeq -0.008 - 0.0008 \sim -0.0088. \quad (4.6)$$

- (3) Since $2|\kappa|/\lambda \simeq 1$, the singlino-dominated $\tilde{\chi}_1^0$ coannihilated with the Higgsino-dominated neutralinos and charginos to provide the measured abundance. In addition, because λ and κ must be small to suppress $C_{\tilde{\chi}_1^0 \tilde{\chi}_1^0 G^0}$ and $C_{\tilde{\chi}_1^0 \tilde{\chi}_1^0 a_s}$, the channels $\tilde{\chi}_1^0 \tilde{\chi}_1^0 \rightarrow t\bar{t}, h_s a_s$ never have a crucial effect on the abundance, even if they are kinematically accessible.

Finally, we investigate the Type-III samples. Figure 1 indicates that some samples correspond to the same parameter space as the Type-II samples, and thus they predict similar DM physics. This conclusion was verified by studying some points in the two scenarios, e.g., points P_2 and P_4 in Table II. In the following, we only concentrate on the samples with same-sign $m_{\tilde{\chi}_1^0}/\mu$ and $\sin 2\beta$. The following results were obtained from Figs. 1 and 4.

- (1) Compared with the Type-II samples, $\lambda v/\mu_{\text{eff}}$ may have a greater value of up to 0.12. The reason is there are accidental cancellations contributing to $\sigma_{\tilde{\chi}_1^0 - p}^{\text{SI}}$, similar to the Type-I samples. This will relax the XENON-1T constraint. We show this characteristic by considering the point P_3 in Table II and finding

$$C_{\tilde{\chi}_1^0 \tilde{\chi}_1^0 h} \simeq 0.047 \times (0.88 - 0.16) + 0.0 - 0.0 \\ + 0.0085 \sim 0.0437, \\ \mathcal{A} \simeq 0.042 - 0.0285 \sim 0.0135.$$

The cancellation also explains why $\sigma_{\tilde{\chi}_1^0 - p}^{\text{SI}}$ was as low as 10^{-50} cm^2 , as shown in the left panel of Fig. 4.

- (2) Due to a relatively large $\lambda v/\mu_{\text{eff}}$ and $|m_{\tilde{\chi}_1^0}/\mu_{\text{eff}}| \rightarrow 1$ in Eq. (2.12), $\sigma_{\tilde{\chi}_1^0 - n}^{\text{SD}}$ may be on the border of 10^{-41} cm^2 (see right panel of Fig. 4). Furthermore, similar to the Type-II samples, $\tilde{\chi}_1^0$ coannihilated with the Higgsino-dominated neutralinos and charginos to achieve the measured abundance.

We add that the point P_3 predicts a significantly larger λ than points P_2 and P_4 . Consequently, this will be readily tested in the near-future PandaX-4T experiments for both SI and SD scattering.

V. CONCLUSION

This work provided updates to previous studies of singlino-dominated DM mainly in four aspects:

- (1) We no longer require the fine-tuning measurement Δm_Z as a model selection criterion, since it may only reflect personal prejudice.
- (2) We adopted an advanced MultiNest algorithm to perform a sophisticated scan over the Z_3 -NMSSM parameter space to ensure that the obtained conclusions were as complete as possible.
- (3) We utilized the latest experimental results to restrict singlino-dominated DM scenarios, including the XENON-1T search for both SI and SD DM-nucleon scattering since 2018, ATLAS analyses of sparticle signals with 139 fb^{-1} of data, and measurements of the Higgs couplings with 80 fb^{-1} of data.
- (4) We provided simplified analytical formulas for both the DM annihilation cross sections and the SI and SD cross sections of DM-nucleon scattering, and we numerically scrutinized each contribution in these formulas.

As a result, a new singlino-dominated DM scenario (Type-I samples) was found. More model information, such as its Bayesian evidence, was obtained, and the current and future statuses of the scenarios were presented. More importantly, this study provided clear insight into singlino-dominated DM scenarios and explained why they had been tightly limited in the Z_3 -NMSSM.

Specifically, this study indicated that the surviving samples can be categorized into three types:

- (1) For Type-I samples, $0.4 \lesssim \lambda \lesssim 0.7$, $0.13 \lesssim \kappa \lesssim 0.23$, $1.5 \lesssim \tan \beta \lesssim 6$, $450 \text{ GeV} \lesssim \mu_{\text{eff}} \lesssim 720 \text{ GeV}$, and the annihilation $\tilde{\chi}_1^0 \tilde{\chi}_1^0 \rightarrow t\bar{t}$ is primarily responsible for the DM abundance.
- (2) For Type-II and -III samples, $0 < \lambda \lesssim 0.15$, $\lambda \simeq 2|\kappa|$, and the dominant annihilation involves a coannihilation with Higgsinos.

The Bayesian evidence (Z) for the three sample types showed that the experiments slightly preferred Type-I samples to Type-II and -III. However, Type-I samples will be examined in the near-future PandaX-4T experiment. They will become highly disfavored if the experiment shows no signs of DM. It should be emphasized that DM annihilation by a singlet scalar or pseudoscalar funnel, a Z -boson funnel, and the SM-like Higgs funnel presented by Abdallah *et al.* [56] were not observed in this study, due to the small Bayesian evidence. In addition, both analytical formulas and numerical results were used to summarize the theory's four primary cases in significantly suppressing the SI scattering cross section for DM-nucleons. This included 1) a small $\lambda v/\mu_{\text{eff}}$, 2) cancellation between $m_{\tilde{\chi}_1^0}/\mu_{\text{eff}}$ and $\sin 2\beta$, 3) cancellation between two contributions from the SM doublet component (H_{SM}) and singlet component (H_s) within the $\tilde{\chi}_1^0 \tilde{\chi}_1^0 h$ coupling strength itself, and 4) cancellation between two contributions from h and h_s .

In summary, the interaction of the singlino-dominated DM with nucleons in the Z_3 -NMSSM has been tightly restricted in current DM-DD experiments, while the measured abundance favors its involvement in weak interactions. Given the theory’s natural preference for electroweak symmetry breaking, it has become increasingly difficult to represent these two seemingly paradoxical features using neutralino DM, due to the limited theoretical structure. Thus, the benefits of singlino-dominated DM are waning unless one extends the Z_3 -invariant theory. Recent studies on the MSSM and NMSSM imply that DM candidates should be gauge singlet fields or that singlet components should at least be naturally dominant over other components [58]. This requirement motivates us to extend the Z_3 -NMSSM to a general NMSSM to increase the Bayesian evidence of the scenarios significantly [88]. It also motivates us to augment the Z_3 -NMSSM with a seesaw mechanism to generate neutrino masses and select the lightest sneutrino as a DM candidate [58,107,115,116].⁸

ACKNOWLEDGMENTS

This work was supported by the National Natural Science Foundation of China (NNSFC) under Grants No. 11575053 and No. 12075076.

APPENDIX: SIMULATION VIA SMOBELS

Recently, the ATLAS Collaboration aimed to limit the compressed mass spectra case. They analyzed 139 fb^{-1} of $\sqrt{s} = 13 \text{ TeV}$ proton-proton collision data collected at the LHC, focusing on the events with missing transverse momentum and two same-flavor, oppositely charged, low-transverse-momentum leptons, further categorizing them by the presence of hadronic activity from initial-state radiation [111]. We repeated this analysis using the simulation tools MadGraph5_aMC@NLO-2.6.6 [121,122] to generate the parton-level events, PYTHIA-8.2 [123] for parton fragmentation and hadronization, DELPHES-3.4.2 [124] for fast simulation of the performance of the ATLAS detector, and CheckMATE-2.0.26 [125–127] to implement the analysis cut selections.

Below, we validate our code for all signal regions (SRs) [111]. We considered $\tilde{l}^+\tilde{l}^-$ production in the MSSM and set the masses of all charginos and neutralinos other than the bino-like $\tilde{\chi}_1^0$ to be 2.5 TeV. Thus, the sleptons will decay by $\tilde{l}^\pm \rightarrow l^\pm \tilde{\chi}_1^0$. We consider the benchmark point $m_{\tilde{l}} = 150 \text{ GeV}$ and $m_{\tilde{\chi}_1^0} = 140 \text{ GeV}$. As a result, the cross section at the next-to-leading order is 126.62 fb for $\tilde{l}_L\tilde{l}_L$ production and 47.62 fb for $\tilde{l}_R\tilde{l}_R$ production. The involved cards were set as follows:

```
import model MSSM.SLHA2 --modelname
generate p p > sl1+ sl1-, (sl1- > e- n1), (sl1+ > e+ n1)
add process p p > sl1+ sl1- j, (sl1- > e- n1), (sl1+ > e+ n1)
generate p p > sl2+ sl2-, (sl2- > mu- n1), (sl2+ > mu+ n1)
add process p p > sl2+ sl2- j, (sl1- > mu- n1), (sl2+ > mu+ n1).
```

For the proc_card.dat:

```
100000 = nevents ! Number of unweighted events requested.
0 = ickkw ! 0 no matching, 1 MLM
37.5 = ktdurham,
```

⁸The properties of the sneutrino DM in the Z_3 -NMSSM were first studied one decade ago [117–120]. However, these studies considered the cases where the cross section of the sneutrino-nucleon scattering was much larger than current DD experimental bounds, so they obtained different conclusions from our work.

For the run_card.dat:

```
Block mass
1000011 1.500000e+02 # Msl1
1000013 1.500000e+02 # Msl2
1000022 1.400000e+02 # Mneu1
1000023 2.500000e+03 # Mneu2
1000024 2.500000e+03 # Mch1
1000025 -2.50000e+03 # Mneu3
1000035 2.500000e+03 # Mneu4
1000037 2.500000e+03 # Mch2
Block selmix
1 1 1.000000e+00 # RR1x1
2 2 1.000000e+00 # RR12x2
4 4 1.000000e+00 # RR14x4
5 5 1.000000e+00 # RR15x5
```

For the param_card.dat and the pythia8_card.dat:

```
Merging:Process = pp>{s11 -,1000011}{s11 +,-1000015}{s12 -,1000013}
{s12 +,-1000013}
Merging:mayRemoveDecayProducts=on
```

In our simulation, we generated 100 000 events for the production process. The results, shown in Table III, indicate that we can reproduce the ATLAS analysis at the 20% level for most cases.

TABLE III. Cut flow for the analysis in Ref. [111]. We considered the point $m(\tilde{\ell}, \tilde{\chi}_1^0) = (150, 140)$ GeV in the calculations.

Process	Production of $\tilde{\ell}\tilde{\ell}$			
Point	$m_{\tilde{\ell}} = 150$ GeV; $m_{\tilde{\chi}_1^0} = 140$ GeV			
Generated Events	100000			
Selection	ATLAS		CheckMATE	
	Events	Efficiency	Events	Efficiency
Total events	24069	...	24069	...
E_T^{miss} trigger	2355.37	...	2355.37	...
Two leptons	1014.55	43.07%	1079.07	45.81%
veto $3 \text{ GeV} < m_{\ell\ell} < 3.2 \text{ GeV}$	1013.21	99.87%	1077.69	99.87%
lepton author 16 veto	1009.48	99.63%	1077.69	100.00%
$\min(\Delta\phi(\text{any jet}, p_T^{\text{miss}})) > 0.4$	970.36	96.12%	1049.11	97.35%
$\Delta\phi(j_1, p_T^{\text{miss}}) > 2.0$	961.15	99.05%	1027.05	97.90%
lepton truth matching	958.99	99.78%	1027.05	100.00%
$1 < m_{\ell\ell} < 60 \text{ GeV}$	827.86	86.33%	883.55	86.03%
$\Delta R_{ee} > 0.3, \Delta R_{\mu\mu} > 0.05, \Delta R_{e\mu} > 0.2$	826.19	99.80%	883.48	99.99%
$p_T^j > 5 \text{ GeV}$	823.70	99.70%	880.95	99.71%
$n_{\text{jet}} \geq 1$	810.59	98.41%	880.95	100.00%

(Table continued)

TABLE III. (Continued)

Process	Production of $\tilde{\chi}^0 \tilde{\chi}^0$			
Point	$m_{\tilde{\chi}^0} = 150 \text{ GeV}; m_{\tilde{\chi}_1^0} = 140 \text{ GeV}$			
Generated Events	100000			
Selection	ATLAS		CheckMATE	
$p_T^{j_1} > 100 \text{ GeV}$	705.86	87.08%	702.58	79.75%
$n_{b\text{-jet}} = 0$	611.05	86.57%	643.78	91.63%
$m_{\tau\tau} < 0 \text{ or } > 160 \text{ GeV}$	533.29	87.27%	569.78	88.51%
ee or $\mu\mu$	532.33	99.82%	569.01	99.86%
SR-highMass				
$E_T^{\text{miss}} > 200 \text{ GeV}$	229.81	43.17%	265.83	46.72%
$\max(0.85, 0.98 - 0.02 \times m_{T_2}^{100}) < R_{\text{ISR}} < 1.0$	160.30	69.75%	165.78	62.36%
$p_T^{\ell_2} > \min(20.0, 2.5 + 2.5 \times (m_{T_2}^{100} - 100))$	70.71	44.11%	72.51	43.74%
$m_{T_2}^{100} < 140 \text{ GeV}$	70.71	100.00%	72.51	100.00%
$m_{T_2}^{100} < 130 \text{ GeV}$	70.71	100.00%	72.51	100.00%
$m_{T_2}^{100} < 120 \text{ GeV}$	70.71	100.00%	72.31	99.73%
$m_{T_2}^{100} < 110 \text{ GeV}$	70.71	100.00%	72.23	99.90%
$m_{T_2}^{100} < 105 \text{ GeV}$	53.72	75.97%	57.10	79.05%
$m_{T_2}^{100} < 102 \text{ GeV}$	20.21	37.62%	23.77	41.63%
$m_{T_2}^{100} < 101 \text{ GeV}$	9.38	46.41%	9.90	41.62%
$m_{T_2}^{100} < 100.5 \text{ GeV}$	4.68	49.89%	4.86	49.11%
SR-lowMass				
$150 < E_T^{\text{miss}} < 200 \text{ GeV}$	146.36	27.49%	167.63	29.46%
$0.8 < R_{\text{ISR}} < 1.0$	107.82	73.67%	93.17	55.58%
$p_T^{\ell_2} > \min(15.0, 7.5 + 0.75 \times (m_{T_2}^{100} - 100))$	52.74	48.91%	42.29	45.39%
$m_{T_2}^{100} < 140 \text{ GeV}$	52.74	100.00%	42.29	100.00%
$m_{T_2}^{100} < 130 \text{ GeV}$	52.74	100.00%	42.29	100.00%
$m_{T_2}^{100} < 120 \text{ GeV}$	52.74	100.00%	42.29	100.00%
$m_{T_2}^{100} < 110 \text{ GeV}$	52.64	99.81%	41.65	98.49%
$m_{T_2}^{100} < 105 \text{ GeV}$	38.05	72.28%	29.09	69.85%
$m_{T_2}^{100} < 102 \text{ GeV}$	16.66	43.78%	11.24	38.62%
$m_{T_2}^{100} < 101 \text{ GeV}$	8.70	52.22%	5.60	49.82%
$m_{T_2}^{100} < 100.5 \text{ GeV}$	4.39	50.46%	2.29	40.88%

[1] G. Aad *et al.* (ATLAS Collaboration), *Phys. Lett. B* **716**, 1 (2012).
 [2] S. Chatrchyan *et al.* (CMS Collaboration), *Phys. Lett. B* **716**, 30 (2012).
 [3] P. A. R. Ade *et al.* (Planck Collaboration), *Astron. Astrophys.* **594**, A13 (2016).
 [4] N. Aghanim *et al.* (Planck Collaboration), *Astron. Astrophys.* **641**, A6 (2020).
 [5] H. E. Haber and G. L. Kane, *Phys. Rep.* **117**, 75 (1985).
 [6] J. F. Gunion and H. E. Haber, *Nucl. Phys.* **B272**, 1 (1986); **B402**, 567(E) (1993).
 [7] H. E. Haber and M. Sher, *Phys. Rev. D* **35**, 2206 (1987).
 [8] U. Ellwanger, C. Hugonie, and A. M. Teixeira, *Phys. Rep.* **496**, 1 (2010).
 [9] M. Maniatis, *Int. J. Mod. Phys. A* **25**, 3505 (2010).
 [10] J. E. Kim and H. P. Nilles, *Phys. Lett.* **138B**, 150 (1984).
 [11] M. Bastero-Gil, C. Hugonie, S. F. King, D. P. Roy, and S. Vempati, *Phys. Lett. B* **489**, 359 (2000).
 [12] L. J. Hall, D. Pinner, and J. T. Ruderman, *J. High Energy Phys.* **04** (2012) 131.
 [13] U. Ellwanger, *J. High Energy Phys.* **03** (2012) 044.

- [14] J. F. Gunion, Y. Jiang, and S. Kraml, *Phys. Lett. B* **710**, 454 (2012).
- [15] S. F. King, M. Mühlleitner, and R. Nevzorov, *Nucl. Phys. B* **860**, 207 (2012).
- [16] D. A. Vasquez, G. Belanger, C. Boehm, J. Da Silva, P. Richardson, and C. Wymant, *Phys. Rev. D* **86**, 035023 (2012).
- [17] J. J. Cao, Z. X. Heng, J. M. Yang, Y. M. Zhang, and J. Y. Zhu, *J. High Energy Phys.* **03** (2012) 086.
- [18] S. F. King, M. Mühlleitner, R. Nevzorov, and K. Walz, *Nucl. Phys. B* **870**, 323 (2013).
- [19] Z. Kang, J. Li, and T. Li, *J. High Energy Phys.* **11** (2012) 024.
- [20] G. Aad *et al.* (ATLAS and CMS Collaborations), *Phys. Rev. Lett.* **114**, 191803 (2015).
- [21] D. Das, U. Ellwanger, and A. M. Teixeira, *J. High Energy Phys.* **04** (2012) 067.
- [22] U. Ellwanger and A. M. Teixeira, *J. High Energy Phys.* **10** (2014) 113.
- [23] U. Ellwanger, *J. High Energy Phys.* **02** (2017) 051.
- [24] U. Ellwanger and C. Hugonie, *Eur. Phys. J. C* **78**, 735 (2018).
- [25] M. Guchait and A. Roy, *Phys. Rev. D* **102**, 075023 (2020).
- [26] E. Aldufeery and M. Binjonaid, *Universe* **7**, 31 (2020).
- [27] H. Baer, V. Barger, P. Huang, and X. Tata, *J. High Energy Phys.* **05** (2012) 109.
- [28] J. Cao, D. Li, L. Shang, P. Wu, and Y. Zhang, *J. High Energy Phys.* **12** (2014) 026.
- [29] J. Cao, Y. He, L. Shang, W. Su, and Y. Zhang, *J. High Energy Phys.* **08** (2016) 037.
- [30] A. M. Sirunyan *et al.* (CMS Collaboration), *J. High Energy Phys.* **11** (2018) 079.
- [31] A. M. Sirunyan *et al.* (CMS Collaboration), *Phys. Lett. B* **790**, 140 (2019).
- [32] A. M. Sirunyan *et al.* (CMS Collaboration), *J. High Energy Phys.* **03** (2018) 160.
- [33] A. M. Sirunyan *et al.* (CMS Collaboration), *Phys. Lett. B* **779**, 166 (2018).
- [34] A. M. Sirunyan *et al.* (CMS Collaboration), *J. High Energy Phys.* **03** (2018) 166.
- [35] A. M. Sirunyan *et al.* (CMS Collaboration), *J. High Energy Phys.* **03** (2018) 076.
- [36] M. Aaboud *et al.* (ATLAS Collaboration), *Eur. Phys. J. C* **78**, 995 (2018).
- [37] M. Aaboud *et al.* (ATLAS Collaboration), *Phys. Rev. D* **100**, 012006 (2019).
- [38] M. Aaboud *et al.* (ATLAS Collaboration), *Phys. Rev. D* **98**, 092012 (2018).
- [39] G. Aad *et al.* (ATLAS Collaboration), *Phys. Rev. D* **101**, 072001 (2020).
- [40] G. Aad *et al.* (ATLAS Collaboration), *Eur. Phys. J. C* **80**, 123 (2020).
- [41] G. Aad *et al.*, *Eur. Phys. J. C* **80**, 691 (2020).
- [42] ATLAS Collaboration, Report No. ATLAS-CONF-2013-035.
- [43] A. M. Sirunyan *et al.* (CMS Collaboration), *Phys. Lett. B* **782**, 440 (2018).
- [44] ATLAS Collaboration, Report No. ATLAS-CONF-2013-093.
- [45] G. Aad *et al.* (ATLAS Collaboration), *J. High Energy Phys.* **05** (2014) 071.
- [46] G. Aad *et al.* (ATLAS Collaboration), *J. High Energy Phys.* **04** (2014) 169.
- [47] G. Aad *et al.* (ATLAS Collaboration), *Eur. Phys. J. C* **75**, 208 (2015).
- [48] CMS Collaboration, Report No. CMS-PAS-SUS-12-022.
- [49] CMS Collaboration, Report No. CMS-PAS-SUS-13-006.
- [50] E. Aprile *et al.* (XENON Collaboration), *Phys. Rev. Lett.* **121**, 111302 (2018).
- [51] E. Aprile *et al.* (XENON Collaboration), *Phys. Rev. Lett.* **122**, 141301 (2019).
- [52] Q. Wang *et al.* (PandaX-II Collaboration), *Chin. Phys. C* **44**, 125001 (2020).
- [53] X. Cui *et al.* (PandaX-II Collaboration), *Phys. Rev. Lett.* **119**, 181302 (2017).
- [54] M. Ackermann *et al.* (Fermi-LAT Collaboration), *Phys. Rev. Lett.* **115**, 231301 (2015).
- [55] J. Cao, Y. He, L. Shang, Y. Zhang, and P. Zhu, *Phys. Rev. D* **99**, 075020 (2019).
- [56] W. Abdallah, A. Chatterjee, and A. Datta, *J. High Energy Phys.* **09** (2019) 095.
- [57] W. Abdallah, A. Datta, and S. Roy, *J. High Energy Phys.* **04** (2021) 122.
- [58] J. Cao, L. Meng, Y. Yue, H. Zhou, and P. Zhu, *Phys. Rev. D* **101**, 075003 (2020).
- [59] U. Ellwanger, G. Espitalier-Noel, and C. Hugonie, *J. High Energy Phys.* **09** (2011) 105.
- [60] F. Feroz, M. P. Hobson, and M. Bridges, *Mon. Not. R. Astron. Soc.* **398**, 1601 (2009).
- [61] F. Feroz, M. P. Hobson, E. Cameron, and A. N. Pettitt, *Open J. Astrophys.* **2**, 10 (2019).
- [62] D. J. C. Mackay, *Information Theory, Inference and Learning Algorithms* (Cambridge University Press, Cambridge, England, 2003).
- [63] J. F. Gunion, D. E. Lopez-Fogliani, L. Roszkowski, R. R. de Austri, and T. A. Varley, *Phys. Rev. D* **84**, 055026 (2011).
- [64] K. Kowalska, S. Munir, L. Roszkowski, E. M. Sessolo, S. Trojanowski, and Y. L. S. Tsai, *Phys. Rev. D* **87**, 115010 (2013).
- [65] D. Kim, P. Athron, C. Balázs, B. Farmer, and E. Hutchison, *Phys. Rev. D* **90**, 055008 (2014).
- [66] L. Roszkowski, S. Trojanowski, and K. Turzyński, *J. High Energy Phys.* **11** (2014) 146.
- [67] P. Athron, C. Balazs, B. Farmer, A. Fowlie, D. Harries, and D. Kim, *J. High Energy Phys.* **10** (2017) 160.
- [68] S. AbdusSalam, *Eur. Phys. J. C* **79**, 442 (2019).
- [69] C. Cheung, M. Papucci, D. Sanford, N. R. Shah, and K. M. Zurek, *Phys. Rev. D* **90**, 075011 (2014).
- [70] J. Cao, L. Shang, P. Wu, J. M. Yang, and Y. Zhang, *J. High Energy Phys.* **10** (2015) 030.
- [71] M. Badziak, M. Olechowski, and P. Szczerbiak, *J. High Energy Phys.* **03** (2016) 179.
- [72] M. Badziak, M. Olechowski, and P. Szczerbiak, *J. High Energy Phys.* **07** (2017) 050.
- [73] S. Baum, M. Carena, N. R. Shah, and C. E. M. Wagner, *J. High Energy Phys.* **04** (2018) 069.
- [74] K. Cheung, T. J. Hou, J. S. Lee, and E. Senaha, *Phys. Rev. D* **82**, 075007 (2010).

- [75] G. Aad *et al.* (ATLAS Collaboration), *Phys. Rev. D* **101**, 012002 (2020).
- [76] A. M. Sirunyan *et al.* (CMS Collaboration), *Eur. Phys. J. C* **79**, 421 (2019).
- [77] U. Ellwanger, J. F. Gunion, and C. Hugonie, *J. High Energy Phys.* **02** (2005) 066.
- [78] G. Belanger, F. Boudjema, C. Hugonie, A. Pukhov, and A. Semenov, *J. Cosmol. Astropart. Phys.* **09** (2005) 001.
- [79] K. Griest and D. Seckel, *Phys. Rev. D* **43**, 3191 (1991).
- [80] M. J. Baker, J. Brod, S. El Hedri, A. Kaminska, J. Kopp, J. Liu, A. Thamm, M. de Vries, X. P. Wang, F. Yu *et al.*, *J. High Energy Phys.* **12** (2015) 120.
- [81] G. Jungman, M. Kamionkowski, and K. Griest, *Phys. Rep.* **267**, 195 (1996).
- [82] A. Pierce, N. R. Shah, and K. Freese, [arXiv:1309.7351](https://arxiv.org/abs/1309.7351).
- [83] L. Calibbi, J. M. Lindert, T. Ota, and Y. Takanishi, *J. High Energy Phys.* **11** (2014) 106.
- [84] G. Jungman, M. Kamionkowski, and K. Griest, *Phys. Rep.* **267**, 195 (1996).
- [85] G. Belanger, F. Boudjema, A. Pukhov, and A. Semenov, *Comput. Phys. Commun.* **180**, 747 (2009).
- [86] M. Drees and M. M. Nojiri, *Phys. Rev. D* **48**, 3483 (1993).
- [87] M. Drees and M. M. Nojiri, *Phys. Rev. D* **47**, 4226 (1993).
- [88] J. Cao, D. Li, J. Lian, Y. Yue, and H. Zhou, [arXiv:2102.05317](https://arxiv.org/abs/2102.05317).
- [89] Q. Riffard, F. Mayet, G. Bélanger, M.-H. Genest, and D. Santos, *Phys. Rev. D* **93**, 035022 (2016).
- [90] M. Badziak, M. Olechowski, and P. Szczerbiak, *Proc. Sci., PLANCK2015* (2015) 130 [[arXiv:1601.00768](https://arxiv.org/abs/1601.00768)].
- [91] U. Ellwanger and C. Hugonie, *Comput. Phys. Commun.* **175**, 290 (2006).
- [92] M. Tanabashi *et al.* (Particle Data Group), *Phys. Rev. D* **98**, 030001 (2018).
- [93] G. Degrassi and P. Slavich, *Nucl. Phys.* **B825**, 119 (2010).
- [94] F. Domingo and U. Ellwanger, *J. High Energy Phys.* **12** (2007) 090.
- [95] F. Domingo, *Eur. Phys. J. C* **76**, 452 (2016).
- [96] G. Belanger, F. Boudjema, A. Pukhov, and A. Semenov, *Comput. Phys. Commun.* **174**, 577 (2006).
- [97] G. Belanger, F. Boudjema, A. Pukhov, and A. Semenov, *Comput. Phys. Commun.* **176**, 367 (2007).
- [98] G. Belanger, F. Boudjema, A. Pukhov, and A. Semenov, *Comput. Phys. Commun.* **185**, 960 (2014).
- [99] G. Belanger, F. Boudjema, A. Goudelis, A. Pukhov, and B. Zaldivar, *Comput. Phys. Commun.* **231**, 173 (2018).
- [100] G. Altarelli and R. Barbieri, *Phys. Lett. B* **253**, 161 (1991).
- [101] G. Altarelli, R. Barbieri, and S. Jadach, *Nucl. Phys.* **B369**, 3 (1992); **B376**, 444(E) (1992).
- [102] G. Altarelli, R. Barbieri, and F. Caravaglios, *Phys. Lett. B* **349**, 145 (1995).
- [103] M. E. Peskin and T. Takeuchi, *Phys. Rev. Lett.* **65**, 964 (1990).
- [104] M. E. Peskin and T. Takeuchi, *Phys. Rev. D* **46** (1992) 381.
- [105] J. Cao and J. M. Yang, *J. High Energy Phys.* **12** (2008) 006.
- [106] J. de Blas, M. Ciuchini, E. Franco, S. Mishima, M. Pierini, L. Reina, and L. Silvestrini, *J. High Energy Phys.* **12** (2016) 135.
- [107] J. Cao, J. Li, Y. Pan, L. Shang, Y. Yue, and D. Zhang, *Phys. Rev. D* **99**, 115033 (2019).
- [108] F. Ambrogio, S. Kraml, S. Kulkarni, U. Laa, A. Lessa, V. Magerl, J. Sonneveld, M. Traub, and W. Waltenberger, *Comput. Phys. Commun.* **227**, 72 (2018).
- [109] S. Kraml, S. Kulkarni, U. Laa, A. Lessa, W. Magerl, D. Proschofsky-Spindler, and W. Waltenberger, *Eur. Phys. J. C* **74**, 2868 (2014).
- [110] C. K. Khosa, S. Kraml, A. Lessa, P. Neuhuber, and W. Waltenberger, [arXiv:2005.00555](https://arxiv.org/abs/2005.00555).
- [111] G. Aad *et al.* (ATLAS Collaboration), *Phys. Rev. D* **101**, 052005 (2020).
- [112] P. Gregory, *Bayesian Logical Data Analysis for the Physical Sciences* (Cambridge University Press, Cambridge, England, 2005).
- [113] H. Jeffreys, in *The Theory of Probability*, 3rd ed. (Oxford University Press, 1961), p. 432.
- [114] H. Zhang *et al.* (PandaX Collaboration), *Sci. China Phys. Mech. Astron.* **62**, 31011 (2019).
- [115] J. Cao, X. Guo, Y. He, L. Shang, and Y. Yue, *J. High Energy Phys.* **10** (2017) 044.
- [116] J. Cao, Y. He, Y. Pan, Y. Yue, H. Zhou, and P. Zhu, *J. High Energy Phys.* **12** (2020) 023.
- [117] D. G. Cerdeno, C. Munoz, and O. Seto, *Phys. Rev. D* **79**, 023510 (2009).
- [118] D. G. Cerdeno and O. Seto, *J. Cosmol. Astropart. Phys.* **08** (2009) 032.
- [119] D. G. Cerdeno, J. H. Huh, M. Peiro, and O. Seto, *J. Cosmol. Astropart. Phys.* **11** (2011) 027.
- [120] D. G. Cerdeño, V. Martín-Lozano, and O. Seto, *J. High Energy Phys.* **05** (2014) 035.
- [121] J. Alwall, R. Frederix, S. Frixione, V. Hirschi, F. Maltoni, O. Mattelaer, H.-S. Shao, T. Stelzer, P. Torrielli, and M. Zaro, *J. High Energy Phys.* **07** (2014) 079.
- [122] J. Alwall, M. Herquet, F. Maltoni, O. Mattelaer, and T. Stelzer, *J. High Energy Phys.* **06** (2011) 128.
- [123] T. Sjostrand, S. Mrenna, and P. Z. Skands, *J. High Energy Phys.* **05** (2006) 026.
- [124] J. de Favereau, C. Delaere, P. Demin, A. Giammanco, V. Lemaître, A. Mertens, and M. Selvaggi (DELPHES 3 Collaboration), *J. High Energy Phys.* **02** (2014) 057.
- [125] D. Dercks, N. Desai, J. S. Kim, K. Rolbiecki, J. Tattersall, and T. Weber, *Comput. Phys. Commun.* **221**, 383 (2017).
- [126] J. S. Kim, D. Schmeier, J. Tattersall, and K. Rolbiecki, *Comput. Phys. Commun.* **196**, 535 (2015).
- [127] M. Drees, H. Dreiner, D. Schmeier, J. Tattersall, and J. S. Kim, *Comput. Phys. Commun.* **187**, 227 (2015).